

AD A 015959

24
B.S.

A TRIDENT SCHOLAR PROJECT REPORT

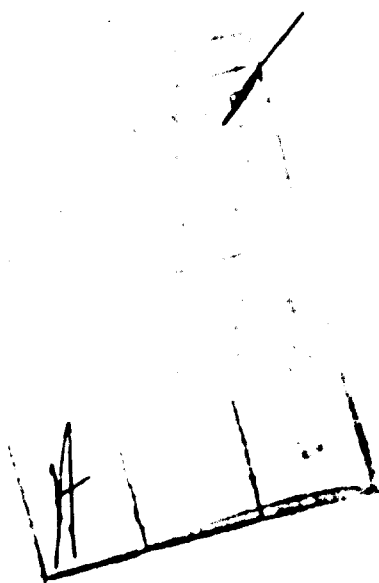
NO. 72

THE ZENITH-ANGLE DISTRIBUTION OF STOPPING
MUONS AT SEA LEVEL, AND THE RESPONSE OF A
STOPPING-MUON COSMIC-RAY DETECTOR



1478
1479
1480
1481
1482
1483
1484
1485
1486
1487
1488
1489
1490
1491
1492
1493
1494
1495
1496
1497
1498
1499
1500
1501
1502
1503
1504
1505
1506
1507
1508
1509
1510
1511
1512
1513
1514
1515
1516
1517
1518
1519
1520
1521
1522
1523
1524
1525
1526
1527
1528
1529
1530
1531
1532
1533
1534
1535
1536
1537
1538
1539
1540
1541
1542
1543
1544
1545
1546
1547
1548
1549
1550
1551
1552
1553
1554
1555
1556
1557
1558
1559
1560
1561
1562
1563
1564
1565
1566
1567
1568
1569
1570
1571
1572
1573
1574
1575
1576
1577
1578
1579
1580
1581
1582
1583
1584
1585
1586
1587
1588
1589
1590
1591
1592
1593
1594
1595
1596
1597
1598
1599
1600
1601
1602
1603
1604
1605
1606
1607
1608
1609
1610
1611
1612
1613
1614
1615
1616
1617
1618
1619
1620
1621
1622
1623
1624
1625
1626
1627
1628
1629
1630
1631
1632
1633
1634
1635
1636
1637
1638
1639
1640
1641
1642
1643
1644
1645
1646
1647
1648
1649
1650
1651
1652
1653
1654
1655
1656
1657
1658
1659
1660
1661
1662
1663
1664
1665
1666
1667
1668
1669
1670
1671
1672
1673
1674
1675
1676
1677
1678
1679
1680
1681
1682
1683
1684
1685
1686
1687
1688
1689
1690
1691
1692
1693
1694
1695
1696
1697
1698
1699
1700
1701
1702
1703
1704
1705
1706
1707
1708
1709
1710
1711
1712
1713
1714
1715
1716
1717
1718
1719
1720
1721
1722
1723
1724
1725
1726
1727
1728
1729
1730
1731
1732
1733
1734
1735
1736
1737
1738
1739
1740
1741
1742
1743
1744
1745
1746
1747
1748
1749
1750
1751
1752
1753
1754
1755
1756
1757
1758
1759
1760
1761
1762
1763
1764
1765
1766
1767
1768
1769
1770
1771
1772
1773
1774
1775
1776
1777
1778
1779
1780
1781
1782
1783
1784
1785
1786
1787
1788
1789
1790
1791
1792
1793
1794
1795
1796
1797
1798
1799
1800
1801
1802
1803
1804
1805
1806
1807
1808
1809
1810
1811
1812
1813
1814
1815
1816
1817
1818
1819
1820
1821
1822
1823
1824
1825
1826
1827
1828
1829
1830
1831
1832
1833
1834
1835
1836
1837
1838
1839
1840
1841
1842
1843
1844
1845
1846
1847
1848
1849
1850
1851
1852
1853
1854
1855
1856
1857
1858
1859
1860
1861
1862
1863
1864
1865
1866
1867
1868
1869
1870
1871
1872
1873
1874
1875
1876
1877
1878
1879
1880
1881
1882
1883
1884
1885
1886
1887
1888
1889
1890
1891
1892
1893
1894
1895
1896
1897
1898
1899
1900
1901
1902
1903
1904
1905
1906
1907
1908
1909
1910
1911
1912
1913
1914
1915
1916
1917
1918
1919
1920
1921
1922
1923
1924
1925
1926
1927
1928
1929
1930
1931
1932
1933
1934
1935
1936
1937
1938
1939
1940
1941
1942
1943
1944
1945
1946
1947
1948
1949
1950
1951
1952
1953
1954
1955
1956
1957
1958
1959
1960
1961
1962
1963
1964
1965
1966
1967
1968
1969
1970
1971
1972
1973
1974
1975
1976
1977
1978
1979
1980
1981
1982
1983
1984
1985
1986
1987
1988
1989
1990
1991
1992
1993
1994
1995
1996
1997
1998
1999
2000
2001
2002
2003
2004
2005
2006
2007
2008
2009
2010
2011
2012
2013
2014
2015
2016
2017
2018
2019
2020
2021
2022
2023
2024
2025
2026
2027
2028
2029
2030
2031
2032
2033
2034
2035
2036
2037
2038
2039
2040
2041
2042
2043
2044
2045
2046
2047
2048
2049
2050
2051
2052
2053
2054
2055
2056
2057
2058
2059
2060
2061
2062
2063
2064
2065
2066
2067
2068
2069
2070
2071
2072
2073
2074
2075
2076
2077
2078
2079
2080
2081
2082
2083
2084
2085
2086
2087
2088
2089
2090
2091
2092
2093
2094
2095
2096
2097
2098
2099
2100
2101
2102
2103
2104
2105
2106
2107
2108
2109
2110
2111
2112
2113
2114
2115
2116
2117
2118
2119
2120
2121
2122
2123
2124
2125
2126
2127
2128
2129
2130
2131
2132
2133
2134
2135
2136
2137
2138
2139
2140
2141
2142
2143
2144
2145
2146
2147
2148
2149
2150
2151
2152
2153
2154
2155
2156
2157
2158
2159
2160
2161
2162
2163
2164
2165
2166
2167
2168
2169
2170
2171
2172
2173
2174
2175
2176
2177
2178
2179
2180
2181
2182
2183
2184
2185
2186
2187
2188
2189
2190
2191
2192
2193
2194
2195
2196
2197
2198
2199
2200
2201
2202
2203
2204
2205
2206
2207
2208
2209
2210
2211
2212
2213
2214
2215
2216
2217
2218
2219
2220
2221
2222
2223
2224
2225
2226
2227
2228
2229
2230
2231
2232
2233
2234
2235
2236
2237
2238
2239
2240
2241
2242
2243
2244
2245
2246
2247
2248
2249
2250
2251
2252
2253
2254
2255
2256
2257
2258
2259
2260
2261
2262
2263
2264
2265
2266
2267
2268
2269
2270
2271
2272
2273
2274
2275
2276
2277
2278
2279
2280
2281
2282
2283
2284
2285
2286
2287
2288
2289
2290
2291
2292
2293
2294
2295
2296
2297
2298
2299
2300
2301
2302
2303
2304
2305
2306
2307
2308
2309
2310
2311
2312
2313
2314
2315
2316
2317
2318
2319
2320
2321
2322
2323
2324
2325
2326
2327
2328
2329
2330
2331
2332
2333
2334
2335
2336
2337
2338
2339
2340
2341
2342
2343
2344
2345
2346
2347
2348
2349
2350
2351
2352
2353
2354
2355
2356
2357
2358
2359
2360
2361
2362
2363
2364
2365
2366
2367
2368
2369
2370
2371
2372
2373
2374
2375
2376
2377
2378
2379
2380
2381
2382
2383
2384
2385
2386
2387
2388
2389
2390
2391
2392
2393
2394
2395
2396
2397
2398
2399
2400
2401
2402
2403
2404
2405
2406
2407
2408
2409
2410
2411
2412
2413
2414
2415
2416
2417
2418
2419
2420
2421
2422
2423
2424
2425
2426
2427
2428
2429
2430
2431
2432
2433
2434
2435
2436
2437
2438
2439
2440
2441
2442
2443
2444
2445
2446
2447
2448
2449
2450
2451
2452
2453
2454
2455
2456
2457
2458
2459
2460
2461
2462
2463
2464
2465
2466
2467
2468
2469
2470
2471
2472
2473
2474
2475
2476
2477
2478
2479
2480
2481
2482
2483
2484
2485
2486
2487
2488
2489
2490
2491
2492
2493
2494
2495
2496
2497
2498
2499
2500
2501
2502
2503
2504
2505
2506
2507
2508
2509
2510
2511
2512
2513
2514
2515
2516
2517
2518
2519
2520
2521
2522
2523
2524
2525
2526
2527
2528
2529
2530
2531
2532
2533
2534
2535
2536
2537
2538
2539
2540
2541
2542
2543
2544
2545
2546
2547
2548
2549
2550
2551
2552
2553
2554
2555
2556
2557
2558
2559
2560
2561
2562
2563
2564
2565
2566
2567
2568
2569
2570
2571
2572
2573
2574
2575
2576
2577
2578
2579
2580
2581
2582
2583
2584
2585
2586
2587
2588
2589
2590
2591
2592
2593
2594
2595
2596
2597
2598
2599
2600
2601
2602
2603
2604
2605
2606
2607
2608
2609
2610
2611
2612
2613
2614
2615
2616
2617
2618
2619
2620
2621
2622
2623
2624
2625
2626
2627
2628
2629
2630
2631
2632
2633
2634
2635
2636
2637
2638
2639
2640
2641
2642
2643
2644
2645
2646
2647
2648
2649
2650
2651
2652
2653
2654
2655
2656
2657
2658
2659
2660
2661
2662
2663
2664
2665
2666
2667
2668
2669
2670
2671
2672
2673
2674
2675
2676
2677
2678
2679
2680
2681
2682
2683
2684
2685
2686
2687
2688
2689
2690
2691
2692
2693
2694
2695
2696
2697
2698
2699
2700
2701
2702
2703
2704
2705
2706
2707
2708
2709
2710
2711
2712
2713
2714
2715
2716
2717
2718
2719
2720
2721
2722
2723
2724
2725
2726
2727
2728
2729
2730
2731
2732
2733
2734
2735
2736
2737
2738
2739
2740
2741
2742
2743
2744
2745
2746
2747
2748
2749
2750
2751
2752
2753
2754
2755
2756
2757
2758
2759
2760
2761
2762
2763
2764
2765
2766
2767
2768
2769
2770
2771
2772
2773
2774
2775
2776
2777
2778
2779
2780
2781
2782
2783
2784
2785
2786
2787
2788
2789
2790
2791
2792
2793
2794
2795
2796
2797
2798
2799
2800
2801
2802
2803
2804
2805
2806
2807
2808
2809
2810
2811
2812
2813
2814
2815
2816
2817
2818
2819
2820
2821
2822
2823
2824
2825
2826
2827
2828
2829
2830
2831
2832
2833
2834
2835
2836
2837
2838
2839
2840
2841
2842
2843
2844
2845
2846
2847
2848
2849
2850
2851
2852
2853
2854
2855
2856
2857
2858
2859
2860
2861
2862
2863
2864
2865
2866
2867
2868
2869
2870
2871
2872
2873
2874
2875
2876
2877
2878
2879
2880
2881
2882
2883
2884
2885
2886
2887
2888
2889
2890
2891
2892
2893
2894
2895
2896
2897
2898
2899
2900
2901
2902
2903
2904
2905
2906
2907
2908
2909
2910
2911
2912
2913
2914
2915
2916
2917
2918
2919
2920
2921
2922
2923
2924
2925
2926
2927
2928
2929
2930
2931
2932
2933
2934
2935
2936
2937
2938
2939
2940
2941
2942
2943
2944
2945
2946
2947
2948
2949
2950
2951
2952
2953
2954
2955
2956
2957
2958
2959
2960
2961
2962
2963
2964
2965
2966
2967
2968
2969
2970
2971
2972
2973
2974
2975
2976
2977
2978
2979
2980
2981
2982
2983
2984
2985
2986
2987
2988
2989
2990
2991
2992
2993
2994
2995
2996
2997
2998
2999
3000
3001
3002
3003
3004
3005
3006
3007
3008
3009
3010
3011
3012
3013
3014
3015
3016
3017
3018
3019
3020
3021
3022
3023
3024
3025
3026
3027
3028
3029
3030
3031
3032
3033
3034
3035
3036
3037
3038
3039
3040
3041
3042
3043
3044
3045
3046
3047
3048
3049
3050
3051
3052
3053
3054
3055
3056
3057
3058
3059
3060
3061
3062
3063
3064
3065
3066
3067
3068
3069
3070
3071
3072
3073
3074
3075
3076
3077
3078
3079
3080
3081
3082
3083
3084
3085
3086
3087
3088
3089
3090
3091
3092
3093
3094
3095
3096
3097
3098
3099
3100
3101
3102
3103
3104
3105
3106
3107
3108
3109
3110
3111
3112
3113
3114
3115
3116
3117
3118
3119
3120
3121
3122
3123
3124
3125
3126
3127
3128
3129
3130
3131
3132
3133
3134
3135
3136
3137
3138
3139
3140
3141
3142
3143
3144
3145
3146
3147
3148
3149
3150
3151
3152
3153
3154
3155
3156
3157
3158
3159
3160
3161
3162
3163
3164
3165
3166
3167
3168
3169
3170
3171
3172
3173
3174
3175
3176
3177
3178
3179
3180
3181
3182
3183
3184
3185
3186
3187
3188
3189
3190
3191
3192
3193
3194
3195
3196
3197
3198
3199
3200
3201
3202
3203
3204
3205
3206
3207
3208
3209
3210
3211
3212
3213
3214
3215
3216
3217
3218
3219
3220
3221
3222
3223
3224
3225
3226
3227
3228
3229
3230
3231
3232
3233
3234
3235
3236
3237
3238
3239
3240
3241
3242
3243
3244
3245
3246
3247
3248
3249
3250
3251
3252
3253
3254
3255
3256
3257
3258
3259
3260
3261
3262
3263
3264
3265
3266
3267
3268
3269
3270
3271
3272
3273
3274
3275
3276
3277
3278
3279
3280
3281
3282
3283
3284
3285
3286
3287
3288
3289
3290
3291
3292
3293
3294
3295
3296
3297
3298
3299
3300
3301
3302
3303
3304
3305
3306
3307
3308
3309
3310
3311
3312
3313
3314
3315
3316
3317
3318
3319
3320
3321
3322
3323
3324
3325
3326
3327
3328
3329
3330
3331
3332
3333
3334
3335
3336
3337
3338
3339
3340
3341
3342
3343
3344
3345
3346
3347
3348
3349
3350
3351
3352
3353
3354
3355
3356
3357
3358
3359
3360
3361
3362
3363
3364
3365
3366
3367
3368
3369
3370
3371
3372
3373
3374
3375
3376
3377
3378
3379
3380
3381
3382
3383
3384
3385
3386
3387
3388
3389
3390
3391
3392
3393
3394
3395
3396
3397
3398
3399
3400
3401
3402
3403
3404
3405
3406
3407
3408
3409
3410
3411
3412
3413
3414
3415
3416
3417
3418
3419
3420
3421
3422
3423
3424
3425
3426
3427
3428
3429
3430
3431
3432
3433
3434
3435
3436
3437
3438
3439
3440
3441
3442
3443
3444
3445
3446
3447
3448
3449
3450
3451
3452
3453
3454
3455
3456
3457
3458
3459
3460
3461
3462
3463
3464
3465
3466
3467
3468
3469
3470
3471
3472
3473
3474
3475
3476
3477
3478

**Best
Available
Copy**



Q

UNCLASSIFIED

Security Classification

DOCUMENT CONTROL DATA R & D

UNCLASSIFIED.

U.S. Naval Academy, Annapolis.

The ZENITH-ANGLE DISTRIBUTION OF STOPPING MUONS AT SEA LEVEL,
AND THE RESPONSE OF A STOPPING MUON COSMIC-RAY DETECTOR.

Research report.

Gordon M. Roesler, Jr.

11 27 May 1975

29.

1.

U.S. Naval Academy - Trident Scholar
project report (U.S.N.A. - TSPR. no. 12)OTHER REPORT NUMBERS: Any other numbers that may be assigned
(this report)This document has been approved for public release;
its distribution is UNLIMITED.

U.S. Naval Academy, Annapolis.

The Zenith-angle distribution of stopping muons at sea level, and the response of a stopping muon cosmic-ray detector were investigated in this research report.

In order to determine the angular response of a wide-angle stopping muon telescope, smaller detectors were placed in coincidence with it, providing a correlation of count rate with zenith-angle of particle arrival. Using numerical integration techniques, computer solutions were employed to predict the zenith-angle-selective count rates for various descriptions of the incident flux. - A least-squares analysis yielded a cosine power $n = 4.7 \pm 0.5$ in the flux expression $I(\theta, \phi) = I_0 \cos^n \theta$.

Employing this flux expression in predictive computer programs provided an accurate model of the wide angle telescope response from which the telescope half-angle was determined. Considerations of overburden effects and data corrections are discussed.

DD FORM 1473

NOV 65

(PAGE 1)

N 0101-807-6801

UNCLASSIFIED.

Security Classification

"The Zenith-Angle Distribution of Stopping Muons
at Sea Level, and the Response of a
Stopping-Muon Cosmic-Ray Detector"

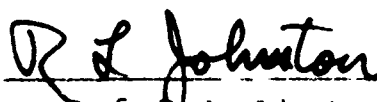
A Trident Scholar Project Report

by

Midshipman Gordon M. Roesler, Jr., Class of 1975

U. S. Naval Academy

Annapolis, Maryland



Advisor: Assoc. Prof. R. L. Johnston, Physics Dept.

Accepted for Trident Scholar Committee



Chairman

22 MAY 1975

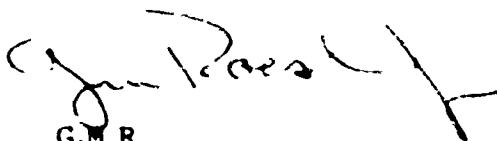
Date

ABSTRACT

In order to determine the angular response of a wide-angle stopping-muon telescope, smaller detectors were placed in coincidence with it, providing a correlation of count rate with zenith angle of particle arrival. Using numerical integration techniques, computer solutions were employed to predict the zenith-angle-selective count rates for various descriptions of the incident flux. A least-squares analysis yielded a cosine power of $n = 4.7 \pm 0.5$ in the flux expression $I(\theta, \phi) = I_0 \cos^n \theta$. Employing this flux expression in predictive computer programs provided an accurate model of the wide angle telescope response from which the telescope half-angle was determined. Considerations of overburden effects and data corrections are discussed.

ACKNOWLEDGMENTS

The author wishes to express his sincere thanks for the friendship and guidance of Drs. Richard Johnston, Frank Miller, and Robert Shelby of the Physics Department, United States Naval Academy. Their ability to convey vast quantities of information in short periods of time, coupled with their understanding and amiability made this project the most profitable and enjoyable experience of his academic career. Also, the talents and patience of Mrs. Jan Harney are warmly appreciated. Her expert typing and her understanding greatly facilitated the production of this work.



G.M.R.
Annapolis, Maryland
12 May, 1975

TABLE OF CONTENTS

<u>Topic</u>	<u>Page</u>
Table of Contents	i
 I. INTRODUCTION	
A. Nature of the Cosmic Radiation Being Investigated	3
B. Detection of Cosmic Rays in General, and of Stopping Muons	6
C. Nature and Purpose of the Experiment	11
 II. APPARATUS	
A. Wide-Angle Stopping-Muon Telescope	14
B. Zenith-Angle Detectors and Mount	16
C. Detectors Used in Efficiency Measurements	22
 III. PREDICTION OF STOPPING-MUON TELESCOPE RESPONSE	
A. The Prediction Problem	23
B. Detector Response by Numerical Integration	24
C. Detector Response by the Trajectory Method	33
 IV. EXPERIMENTAL DETERMINATION OF ZENITH-ANGLE DISTRIBUTION	
A. Collection of Data	37
B. Detection Efficiency of Zenith-Angle Detectors	38
C. Statistical Error Calculation	40
D. Shower Corrections	42
E. Correlated-Pulsing Corrections	45
F. Compensation for Counting Efficiency of Muon Telescope Components	48
G. Positional Error of Zenith-Angle Detectors	52
 V. COMPARISON OF MEASURED DATA AND PREDICTED RESPONSE	
A. The Chi-Square Fit	53
B. Analysis of Data	56

TABLE OF CONTENTS (Cont'd)

VI. DISCUSSION OF RESULTS

A. Mathematical Description of Detector System	61
B. Description of the Stopping-Muon Flux at Sea Level	63
C. Energy Considerations	64
D. Suggestions for Further Research	67
 TABLE 1	 70
 TABLE 2	 71
 TABLE 3	 72
 TABLE 4	 73
 TABLE 5	 74
 LITERATURE CITED	 75
 APPENDIX A	 77
 APPENDIX B	 81
 APPENDIX C.....	 89
 APPENDIX D	 94

I. INTRODUCTION

A. Nature of the Cosmic Radiation Being Investigated

Ever since the discovery of cosmic radiation at the beginning of this century, men have attempted to answer several questions concerning it. The significant problems in cosmic-ray astronomy require the disciplines of astronomy, astrophysics, particle physics, and even meteorology, in order to answer them. Such questions as these are asked:

Where do cosmic rays originate?

What mechanisms produce and accelerate them?

What happens to cosmic rays in their transit of deep space?

How do they interact with the earth's atmosphere?

Of what particles are they composed?

How may cosmic rays be detected and counted accurately?

If these questions are examined in reverse order, it becomes apparent that a good deal of extrapolation is required to utilize data collected at the earth's surface if events in deep space are to be analyzed. This extrapolation is complicated by the interactions of cosmic rays with the earth's atmosphere, and with the geomagnetic and heliomagnetic fields.

A diagrammatic description of cosmic radiation is shown in Figure 1. Measurements taken directly in the primary region indicate that the primaries are basically isotropic above the horizon⁽¹⁾, and are composed mainly of highly energetic nuclei, especially protons. A more complete description of the primary atomic abundances is contained in Table I⁽²⁾. In addition to these fast nuclei, the primary radiation contains some neutrinos and energetic gamma rays.

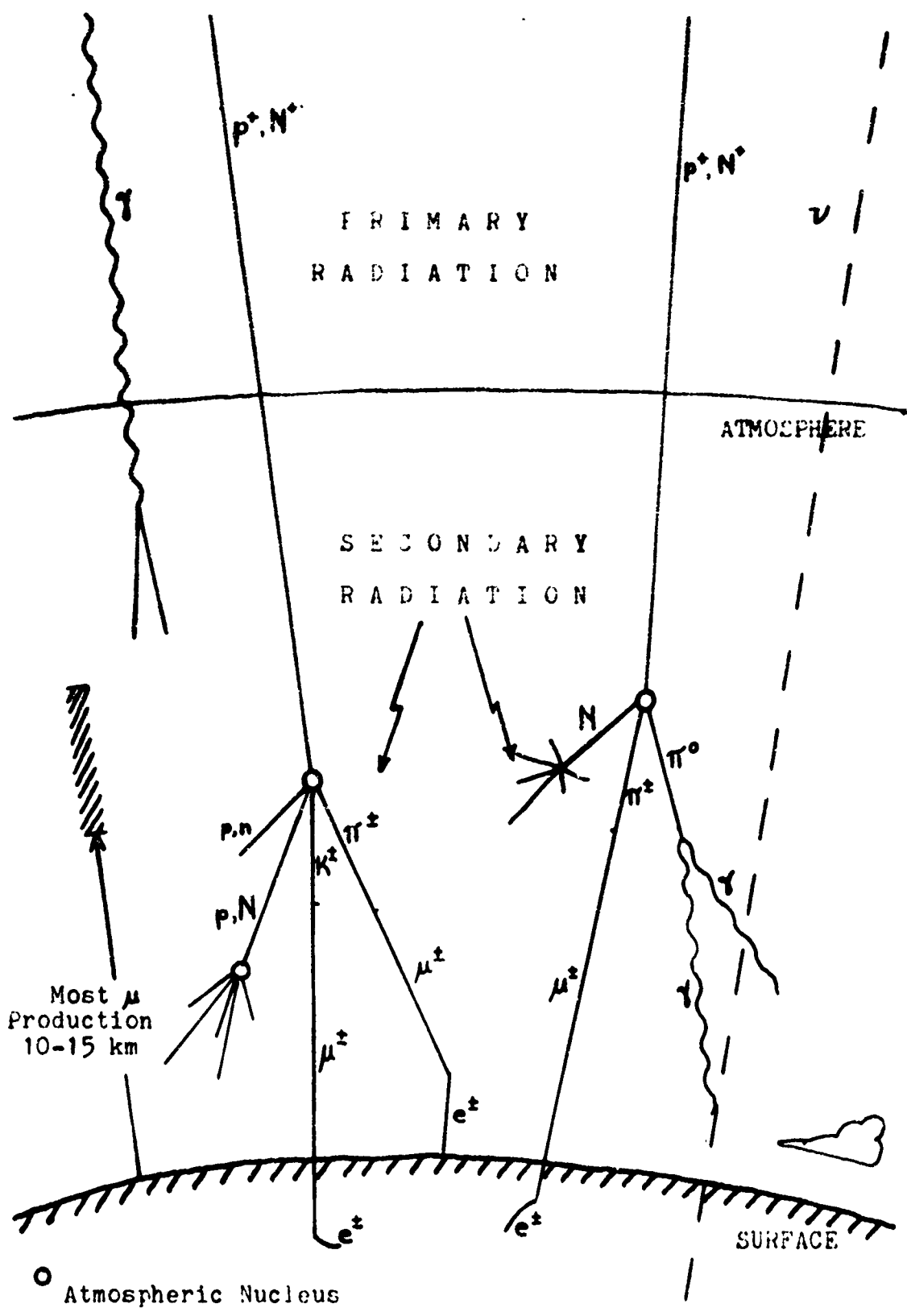


Figure 1. Examples of cosmic ray interactions with the atmosphere.

Of the secondary cosmic rays surviving at the earth's surface, by far the most plentiful constituents are photons, electrons, and muons. The photons and electrons comprise the "soft" component, which is separable from the "hard" component by shielding with approximately six inches of lead. The hard component is almost exclusively muons, with protons and pions comprising only one-half percent of the hard radiation^(1,4).

The nature and properties of the muon are rather well-known. It is an unstable particle with a half-life of about 1.6 microseconds, and has a mass of about 105.6 MeV. It is born in the decay of two unstable fragments of a nuclear explosion in the upper atmosphere, caused by the impact of a primary particle upon a nucleus of the atmosphere. These two fragments, the charged pion and the kaon, decay as follows⁽¹⁾:

$$\pi^{\pm} \rightarrow \mu^{\pm} + \nu$$

with a half-life of 26 nanoseconds, and

$$K^{\pm} \rightarrow \mu^{\pm} + \nu$$

with a half-life of about 12 nanoseconds. K^{\pm} and π^{\pm} represent charged kaons and pions, respectively, the parent particles of virtually all muons in cosmic radiation^(6,7,p.171). The pion decay scheme is virtually one hundred percent probable, and the kaon scheme, about sixty percent⁽⁵⁾.

The majority of muon production takes place in the region of the atmosphere ten to fifteen kilometers above the earth's surface^(6,p.176).

The extremely short-lived pions and kaons decay in flight, but muons have some probability of reaching the earth's surface, aided greatly by the relativistic time dilation for fast particles. The survival probability of the muon is dependent not only on this decay probability, but also on the amount of energy it has, which is decreased by ionization loss in its transit through the atmosphere.

Should the muon be brought to rest before it decays, it will remain virtually noninteracting until its decay. Whether this event occurs in air, rock, or inside a detector, the decay follows the reaction

$$\mu^+ \rightarrow e^+ + \nu$$

with a half-life of about 1.6 microseconds. As shall be seen later, this decay can be useful in identifying a particle as a muon. Figure 2 diagrams the flight of two muons, one of which has so much energy that it penetrates deep into the earth's crust, and the other having just enough energy to penetrate and stop within a "detector" at the earth's surface.

The stopping muon is the particle with which this experiment is uniquely concerned.

B. Detection of Cosmic Rays in General, and of Stopping Muons

The first detections of cosmic rays were made with electroscopes, which were found to lose charge anomalously to the atmosphere^(6,p.2). The identification of the cause of charge loss as ionizing radiation was first accomplished with cloud chambers; later, photographic

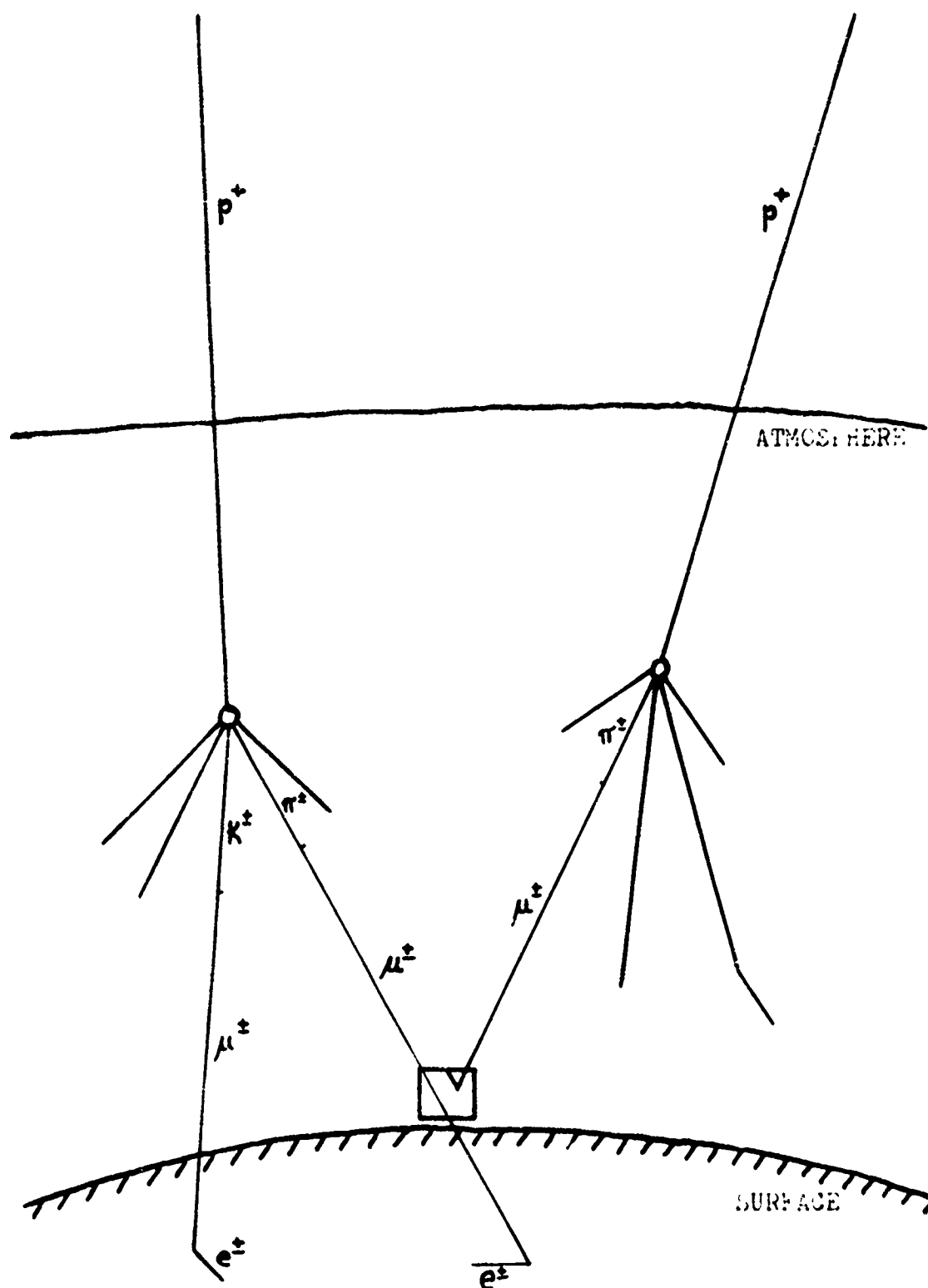


Figure 4. Two muon-producing cosmic ray interactions.

emulsions, spark chambers, and bubble chambers were used to make visible their flights and their interactions with matter. Once they were positively identified as charged particles of various kinds, the detection problem became one of detecting them efficiently, cheaply, and in large numbers without excessive random error. The first detector used for this purpose was the well-known Geiger counter.

Another detection method, the only one employed in this experiment, employs scintillating materials. The same ionization which triggers a Geiger tube causes a scintillator to emit a small flash of light, the amplitude of the light pulse being proportional to the amount of energy lost by the particle through ionization. This light pulse is detected by a photomultiplier tube, whose output is an electrical pulse caused by the photoelectric effect with subsequent amplification. Scintillating materials are of many types, but the scintillator used exclusively in this experiment is a transparent plastic, much like plexiglas, which has been doped with a chemical scintillator.

Electronic coincidence circuitry provides the means whereby different combinations of detectors may be used in cosmic ray detection and selectivity. The principle of coincidence logic is illustrated in Figure 3, a diagram of a hypothetical cosmic-ray telescope. P_1 , P_2 , P_3 and P_4 could be trays of Geiger tubes, or they could be sheets of scintillating plastic with attached photomultiplier tubes. A coincidence between any two of them could indicate that a cosmic ray had transited them, or it could have been a randomly-generated coincidence, called an accidental. Two separate cosmic rays arriving simultaneously, or noise pulses appearing as cosmic rays, can cause accidentals; the

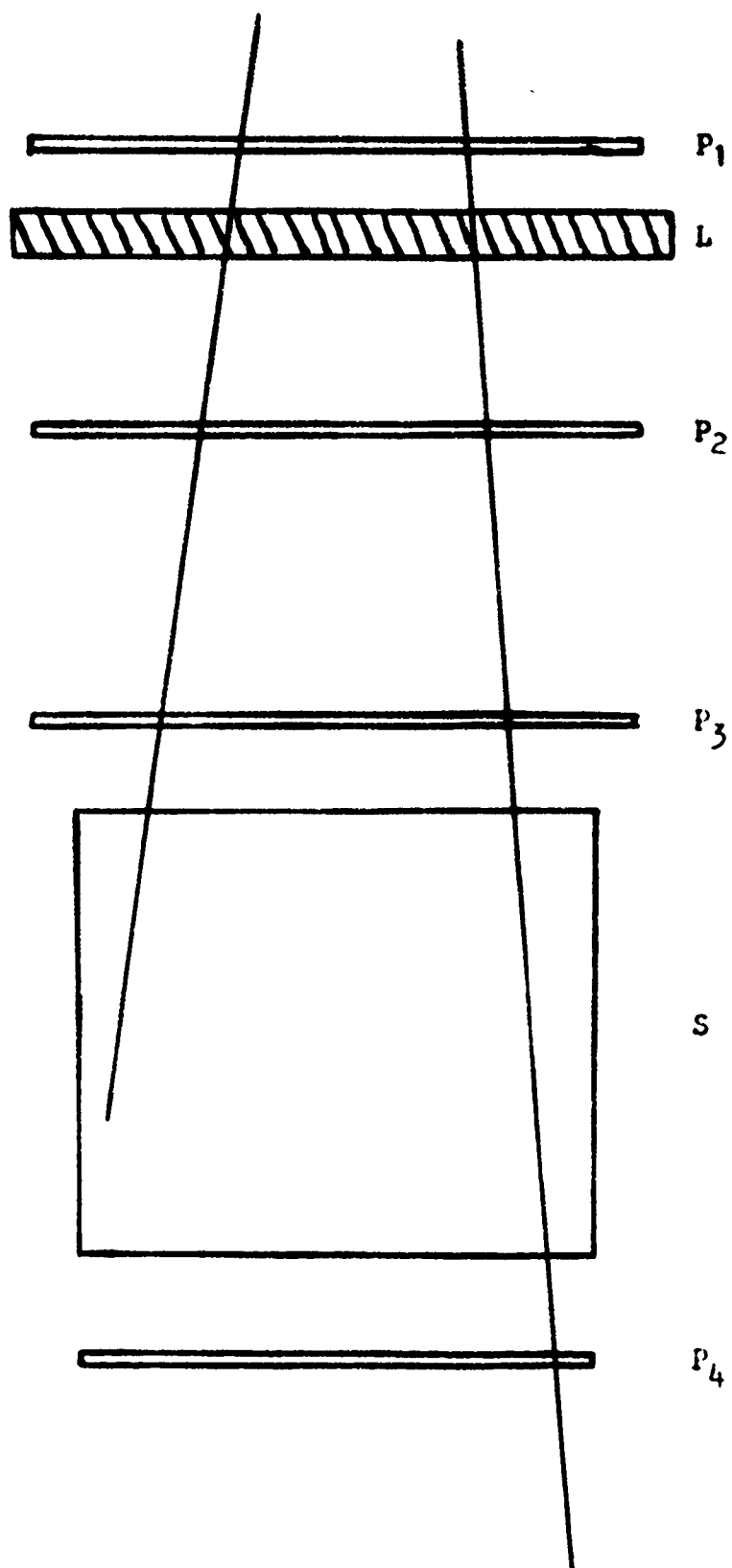


Figure 3. Detector arrangement illustrating the principle of coincidence counting.

more coincidences that are required for the event signature, however, the less likely such accidentals should be, since the upper bound on accidental counts is given

$$R_{\text{acc}} = T_r^{n-1} R_1 R_2 \cdots R_n$$

where T_r is the resolving time of the coincidence circuitry (typically a fraction of a microsecond), and the R_i 's are the count rates for each detector by itself. The event $P_1 P_2 P_3 P_4$ has very little probability of being an accidental, and would be interpreted as a through cosmic ray.

Anticoincidence measurements can be equally valuable. The event $P_1 P_2 P_3 \bar{P}_4$, where the bar indicates the absence of a coinciding pulse, signifies a cosmic ray which has transited the top three plates, but which stopped before reaching the lowest plate. S could be a spark chamber, a cloud chamber, a mass of scintillating plastic for analyzing muon decay, or simply a mass of lead. L, a slab of lead, is often used to eliminate the soft component of radiation from a telescope of this sort.

Two properties of muons are useful in detecting them uniquely in the cosmic ray flux. First, all muons interact only weakly with nuclei, and thus can transmit large thicknesses of shielding without being stopped. As a matter of fact, much cosmic-ray research is carried out deep underground, in order to insure the purity of the muon component. Also, the muon decay into an electron may be employed to give the muon a unique signature. The latter method is of importance in this experiment. When a muon is stopped by ionization loss within a mass

of scintillator, two pulses will be observed by the viewing phototubes: the first pulse from the muon itself, the second pulse from its decay electron. As an added benefit, the time differences between a large number of these pulse pairs should correspond to the muon decay curve, i.e., should represent a radio-active decay with a half-life of 1.6 microseconds.

Thus one signature of a stopping muon could be the observation of a stopping particle via coincidence and anticoincidence techniques, followed by a delayed pulse seen only in the stopping region.

C. Nature and Purpose of the Experiment

A wide-angle stopping-muon telescope has been maintained under the auspices of the Physics Department of the United States Naval Academy, and as of this writing has been collecting data for approximately two and one-half years. Figure 4 indicates the major components of the telescope. It consists of a coincidence scintillator plate, a scintillating stop tank, and an anticoincidence plate to fulfill the stopping signature. The purposes of this experiment were to determine the angular response of this detector, and to determine an expression for the stopping-muon flux within and outside the surrounding building.

Knowing the detector response as a function of zenith angle would provide knowledge of the number of particles arriving from the north and south of zenith, a measure of the segment of the celestial sphere actually being observed. It would, in addition, be an exact measure of the expected time-width of a narrow unfocused source on the

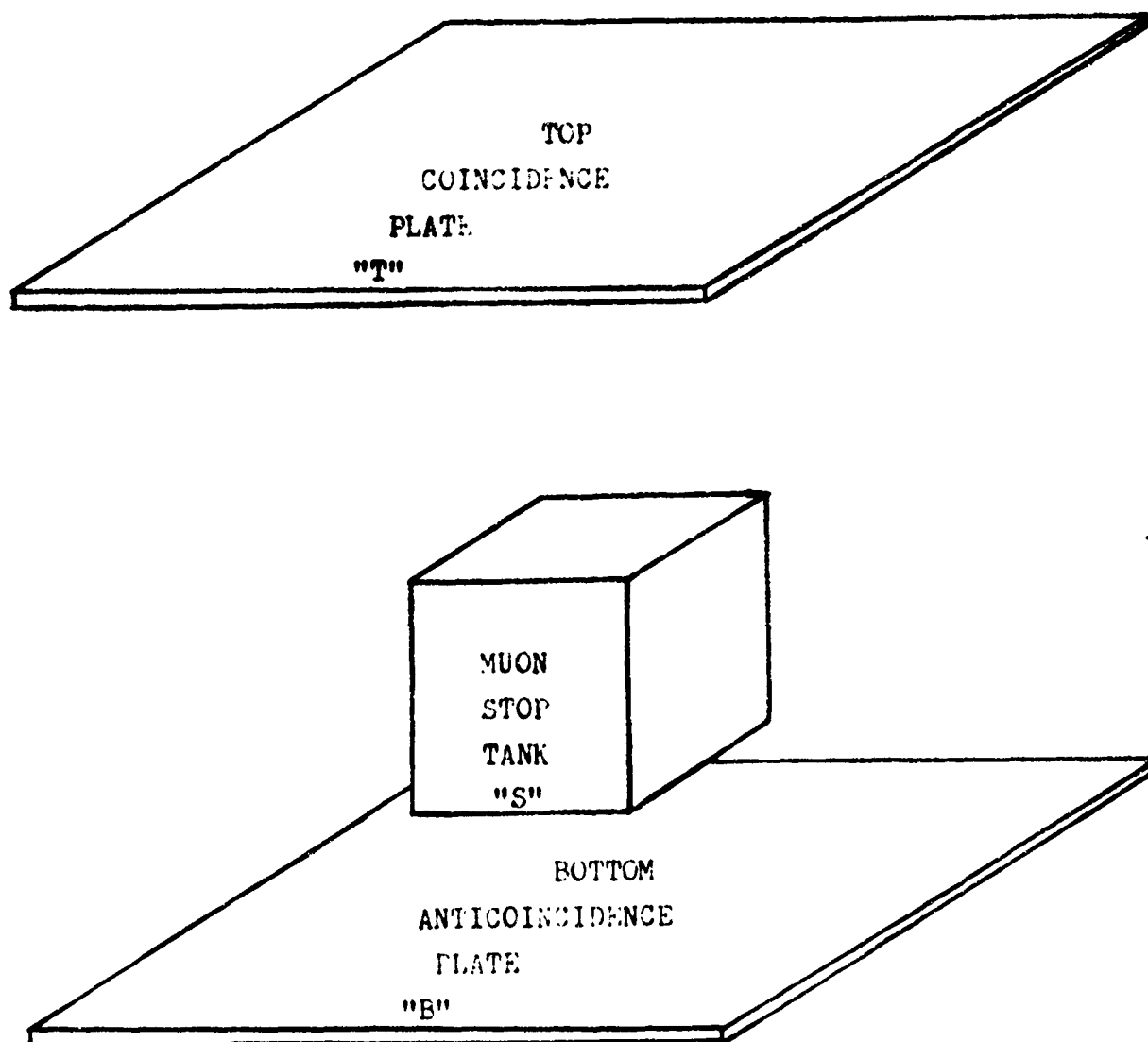


Figure 4. Major scintillator components of stopping-muon telescope.

celestial sphere, since the telescope is rotated by the earth in a west-east direction. Knowing the actual distribution of stopping muons at sea level would be an excellent test of the weaknesses of various muon-production models that have been developed elsewhere.

The measured response of the detector at various zenith and azimuth angles, obtained by using narrow-angle detectors as additional coincidence units to define the arrival directions of the muons, was to be compared to computer programs which predicted this response. Since different predictions of the measured response would be generated for different assumed fluxes, curve-fitting techniques were employed to determine the best descriptions, both of the flux and of the detector response.

Secondarily, the stopping-muon distribution obtained was to be compared with differential fluxes measured by other authors. This was to give an indication of detector efficiency, of the correctness of the flux expression, and of the effects of the building upon the measurements.

II. APPARATUS

A. Wide-Angle Stopping-Muon Telescope

Figure 5 shows a more detailed schematic view of the wide-angle stopping-muon telescope, the angular response of which was to be determined. Each of the 48" x 48" scintillator plates was viewed by four RCA 56 AVP 2" photomultiplier tubes, operated independently of one another. The light-tightness of these plates was maintained by aluminum sheets on their top and bottom faces, and black polyethylene around the edges. The muon stop tank consisted of fifteen 1" thick scintillator plates, each 16 3/4" x 16 3/4", stacked sideways, with one 3/4" thick light pipe on each end. The light-tight box surrounding the scintillator was constructed of black-painted 3/4" plywood. The stop tank was viewed by two Amperex XP 1040 5" photomultiplier tubes operated in coincidence.

The signature required to classify an event as a stopping muon was a TSB coincidence, followed by an STB coincidence between 0.3 μsec and 5.0 μsec later. The TSB pulse was also used as the start pulse for an LRS time-to-pulse amplitude converter, and the STB as the stop pulse. The time-to-amplitude converter provided time-scaled output pulses to a Kicksort multichannel analyzer. The distribution of pulse pairs with respect to time interval was expected to correspond to the muon decay distribution. The multichannel analyzer accumulation was also used as a check on the ability of the system to separate true muon counts from noise-generated counts.

The 2" photomultiplier tubes were operated at 2200 V. The 5" tubes were operated at 2300 V for part of the experiment, and at 2200 V

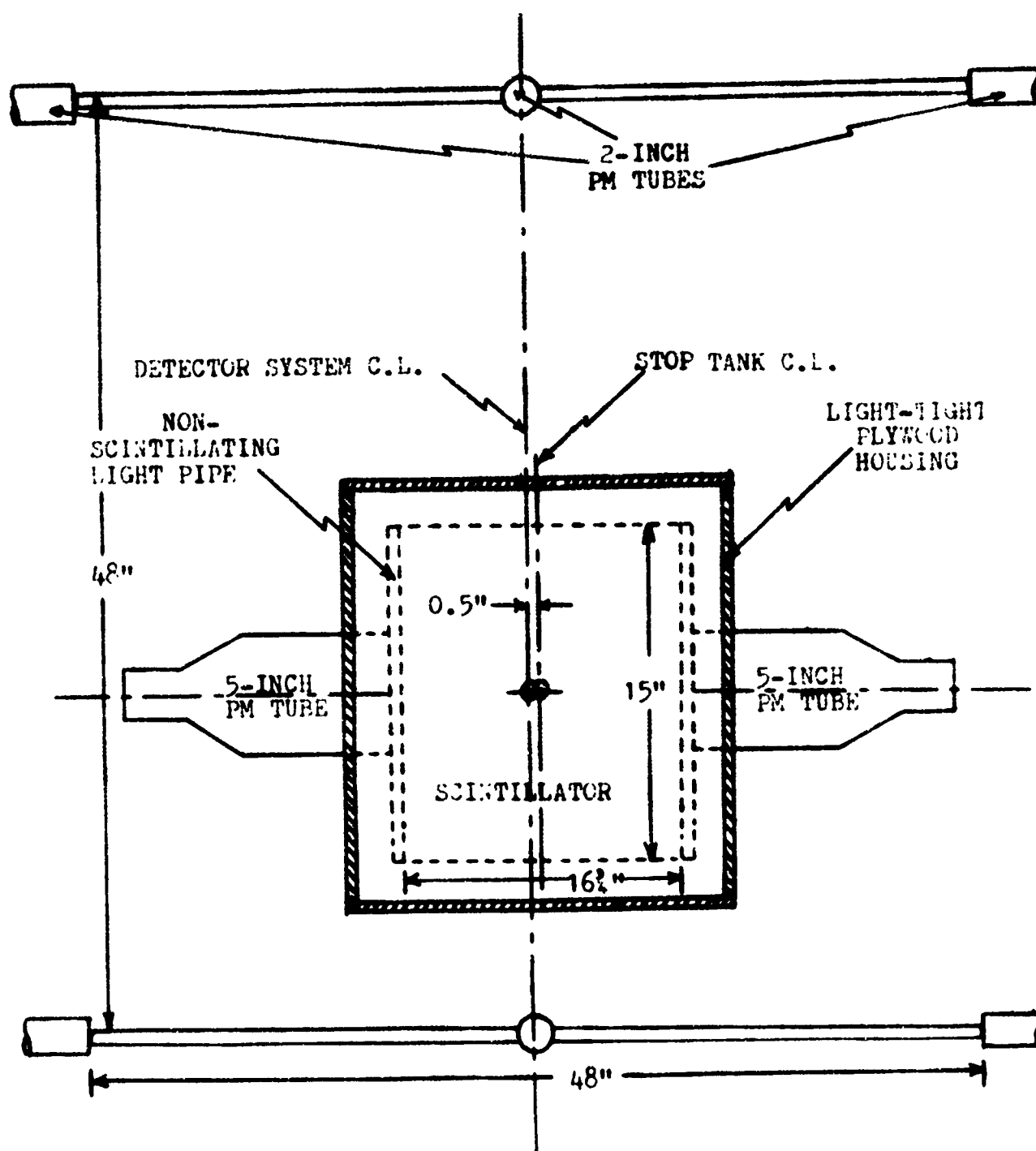


Figure 5. Detail of stopping-muon telescope, looking east (structural details excluded).

thereafter (see Section IV E.) The top and bottom plates' tubes were supplied from a high-voltage supply separate from that for the stop-tank tubes, effecting electrical isolation. Appendix A contains the complete block-diagram circuitry for the stopping-muon counting system.

B. Zenith-Angle Detectors and Mount

Figure 6 shows a disassembled view of one of six zenith-angle detectors, three of which were used in the measurement of the response of the wide-angle detector. The two scintillator discs were separated from the photomultiplier tube by a non-scintillating plastic disc in order to reduce ringing in the tube from large-amplitude light flashes. The scintillator was wrapped in aluminum foil to enhance light collection efficiency. The single Amperex XP 1000 2" photomultiplier was operated at 1600 V, the power supply being separate from the stop tank supply and the top and bottom plate supply.

The basic probes themselves had been constructed previously, for use in another experiment. When this experiment was commenced, each phototube was optically recoupled to the light pipe using Dow-Corning 20-057 Optical Coupling Compound. The masonite-aluminum joints were sealed with electrical tape, and the probes were tested for light-tightness and correct amplitude-response curve. A wooden "key", measuring 4" x 8" x 3/4", was added to the scintillator end of each probe, for mating with the radial zenith-angle mount.

The zenith-angle mount was designed and built subject to the following considerations: that the detectors it supported should be

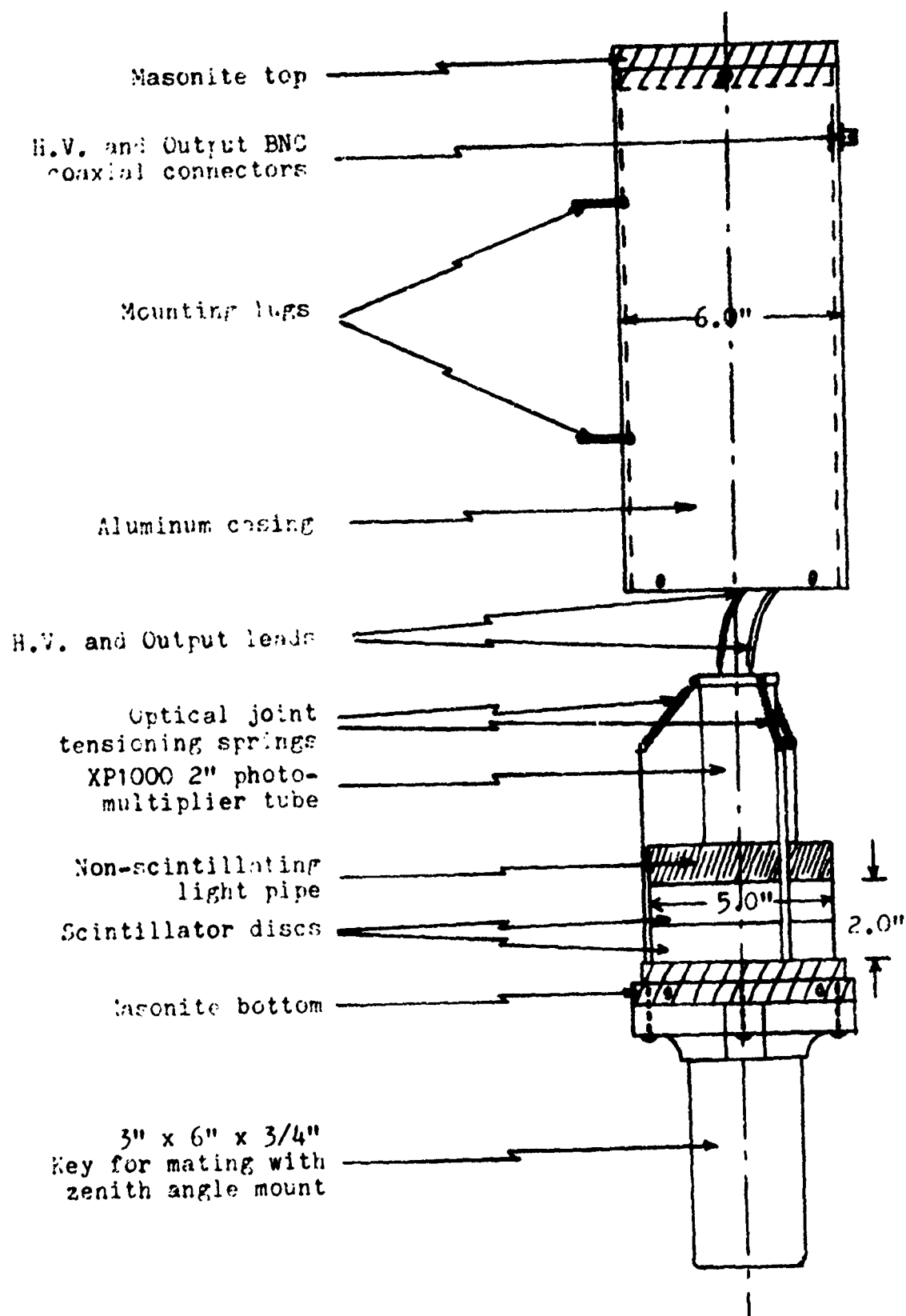


Figure 6. Exploded view of zenith-angle detector.

equidistant from the stop tank center; that they should be able to be positioned anywhere up to the limits of the muon telescope's viewing angle; and that measurements should be available in the north-south plane, the east-west plane, and selected diagonal planes. The main structural elements of the mount are four plywood arcs, of radius 60.0", which are fastened together in pairs at maple slot boards every ten degrees of arc. These maple slot boards also support the zenith-angle detectors. The two arc pairs are slotted in order to mate into four perpendicular arms. A fifth arm, also of radius 60" but of only half the length, was designed for positioning in planes along a diagonal azimuth. Figure 7 shows an orthogonal view of one mount arc, and Figure 8 is a perspective view of the assembled mount with diagonal arm.

The original design of the mount called for resting it directly on the top coincidence plate of the muon telescope. However, in order to clear the phototubes on the edges of the top plate, part of the bottom of each arm was removed, causing the depth of recess to be only 6", and the assembled mount was rested on four cement blocks turned edgewise, placing the recess approximately 7.5" above the top plate.

Figure 9 is a schematic representation of the entire detection system. The automatic data readout system printed out five separate counts every thirty minutes, namely:

- TB, the through cosmic ray rate;
- $TS\bar{B} * S\bar{T}\bar{B}$, the stopping muon rate;
- $2_4TS\bar{B} * S\bar{T}\bar{B}$, $2_9TS\bar{B} * S\bar{T}\bar{B}$, and $2_{15}TS\bar{B} * S\bar{T}\bar{B}$, the

three zenith-angle-selective stopping muon rates. The asterisk represents the delayed coincidence requirement. The subscripts 4, 9, and 15

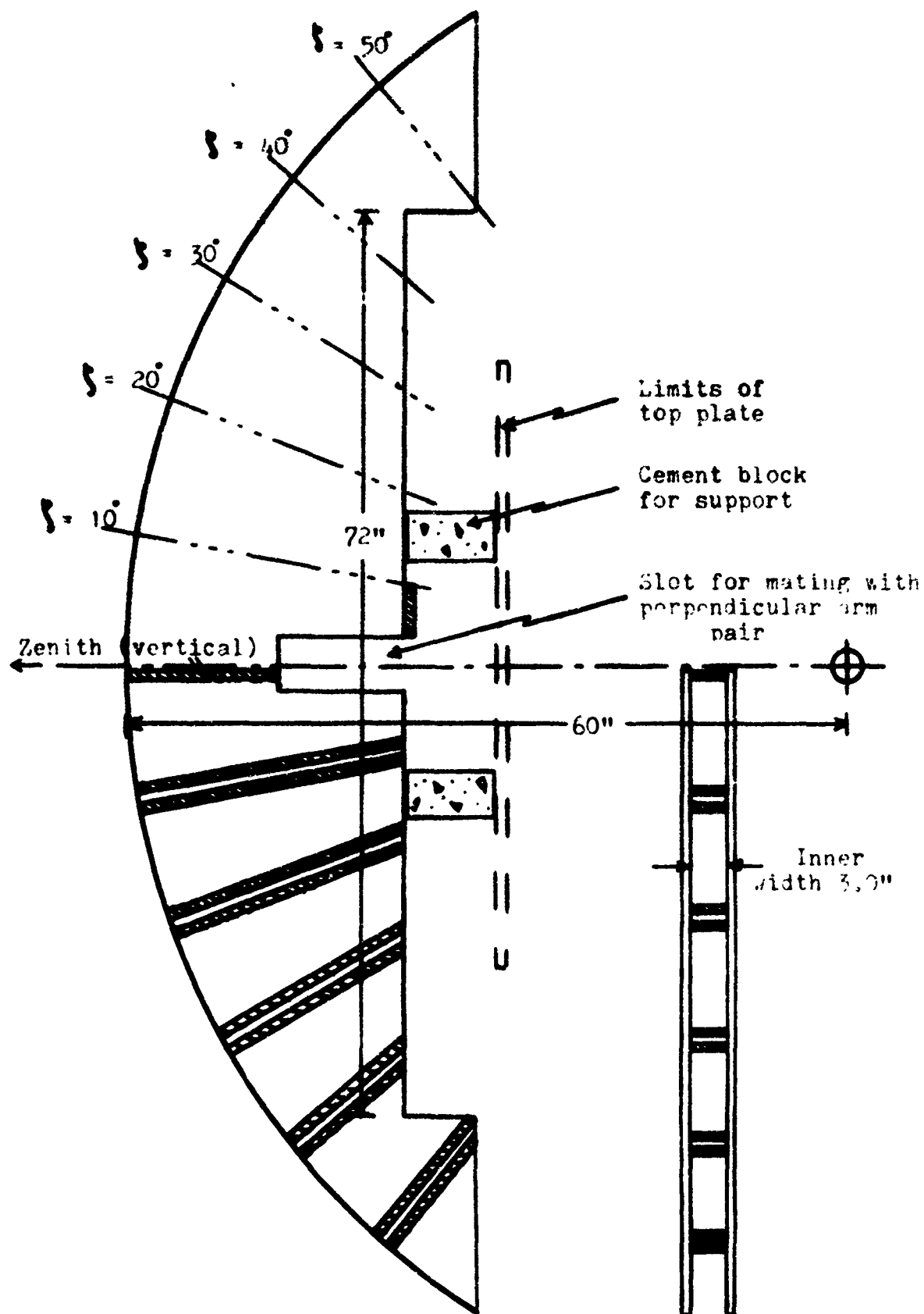


Figure 7. 60-inch zenith-angle mount, orthogonal projection.

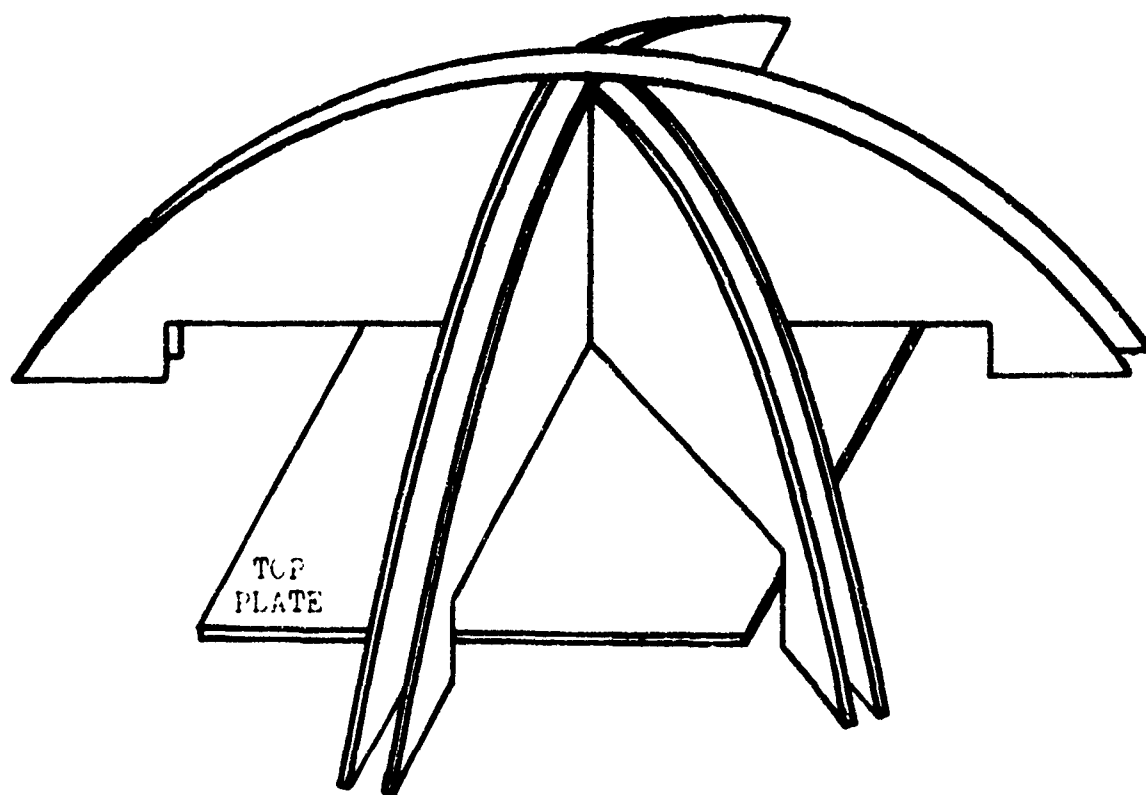


Figure 8. Assembled zenith-angle mount with single arm installed, foreshortened view. (Slots not shown.)

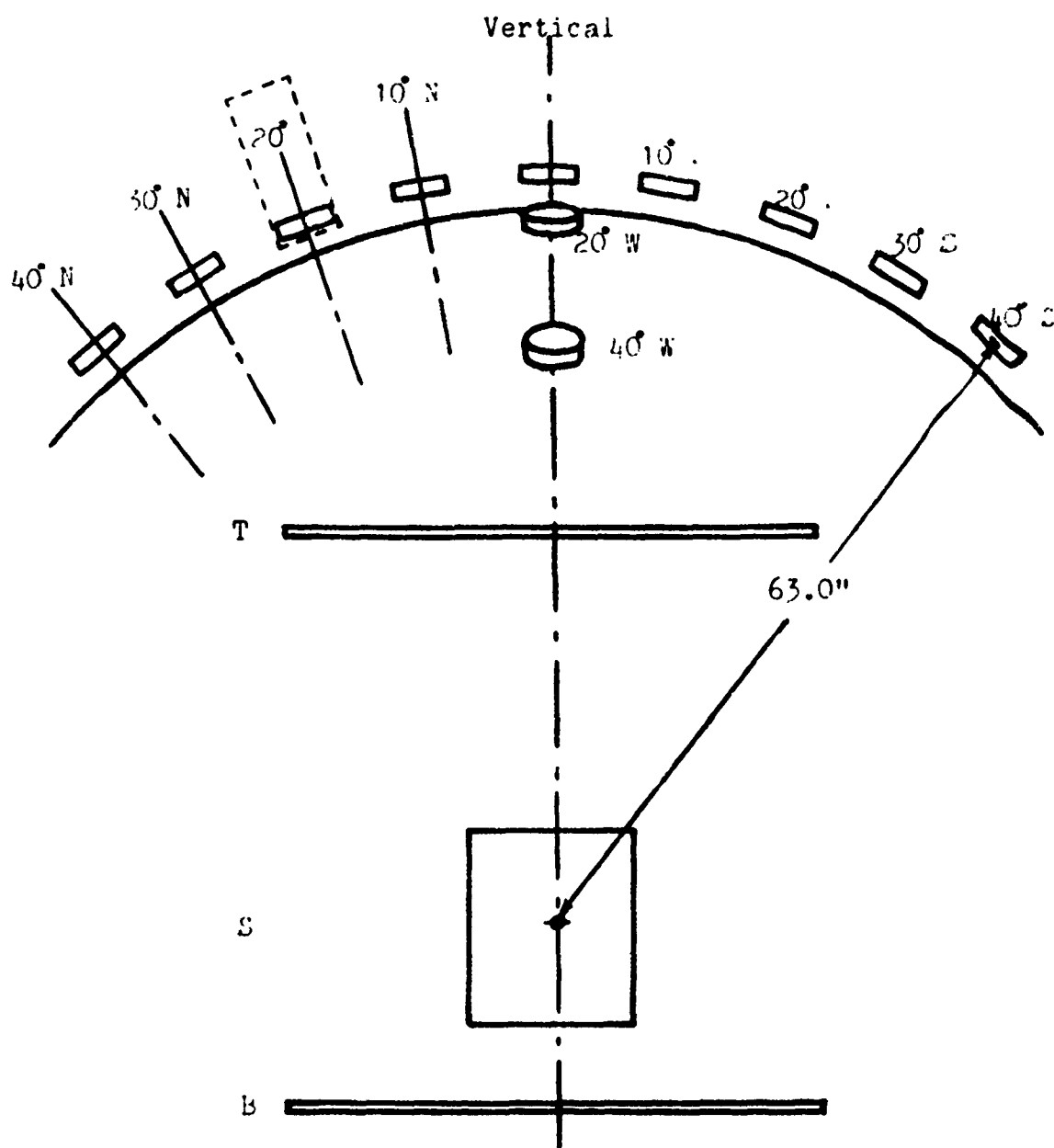


Figure 9. Schematic representation of zenith-angle-selective stopping-muon counting system. (looking east)

are merely labels which identify particular zenith-angle detectors and their associated electronics.

The dimensions of the detector system are listed in Table 2. The predictive computer programs explained in Sections III A and III B are based on these dimensions. One of the first discoveries made during this experiment was the offset of the stop tank of 0.5" from the center of the detection system defined by the top and bottom plates. This turns out to have a significant effect on the count rate of a zenith-angle detector at the 40° N and 40° S positions.

C. Detectors used in Efficiency Measurements

Two small detectors were employed to measure the efficiency of various system components. One was a 4" x 4" x 3/4" single scintillator, viewed on its face by an XP 1000 phototube. The other consisted of two stacked 6" x 6" x 3/4" scintillator plates, viewed on edge by one XP 1000 phototube. Each tube was separated from the scintillator by a 1/4" thick non-scintillating Lucite light pipe. Light-tightness was provided by electrical tape and black polyethylene sheet. Springs were used on the 6" detector to maintain pressure on the optical joint, and its scintillating plates were wrapped in aluminum foil to enhance light collection efficiency.

III. PREDICTION OF STOPPING-MUON TELESCOPE RESPONSE

A. The Prediction Problem

One may make an analogy between the problem of predicting a detector's response to an unknown flux, and a boy shooting marbles into a rink. The unknown quantities are the number and rate of marbles which the boy shoots in each direction, and the number that arrive in the rink. One could place cups within the rink for a uniform length of time, retrieve them, and count the marbles within them, obtaining a rate distribution over the area of the rink. This data could be used in summation to yield the number of marbles falling within the rink. In a second approach, knowing the boy's distance from the rink, some sample paths of marbles could be examined to see if they fall within the rink, and to see how long the allowed stopping distance is for each. This approach may seem less direct compared to the former; but its results predict the marbles landing in the rink for each path individually, without dependence on the width of a cup's mouth.

In the analogy, a very complicated rink represents the wide-angle stopping-muon telescope; the marbles are muons; and the cups model the zenith-angle detectors. The correlation of stopping-muon flux to angular response was to be accomplished using the zenith-angle detectors in coincidence with the muon telescope as a whole. The mobility of the zenith-angle detectors would allow them to cover, over a period of several months, the entire viewing aperture of the muon telescope. The expected count rate from such an arrangement was to be predicted by a numerical integration scheme by computer. The rate predictions

of this scheme depended upon the mathematical description of the detector geometry, just as an estimate of the number of marbles each cup would collect would depend upon its position within the rink.

The rate predictions for the zenith-angle detectors were to be obtained for several flux distributions. By curve-fitting, the flux distribution yielding the closest match of predicted and observed count rates was deemed to be the extant distribution within the surrounding building. An analysis of the wide-angle telescope's response could then be performed either by numerical integration or by the "trajectory" method. The latter method is actually a pseudo-Monte Carlo technique, which determines for many particle trajectories whether or not each meets the geometrical criteria for detection.

All of these predictive processes involved iterative schemes, which were programmed on the Honeywell 635/Dartmouth Time-Sharing System at the United States Naval Academy, in programs using the BASIC language.

B. Detector Response by Numerical Integration

Figure 10 depicts the two-detector problem variables. For two elemental detector areas dA_1 and dA_2 , which are separated by the vector \vec{r}_{12} , and whose normals \hat{N}_1 and \hat{N}_2 make angles θ_1 and θ_2 with \vec{r}_{12} , the absolute count rate seen by these detectors in coincidence will be

$$dR = I \epsilon_1 \epsilon_2 (dA_2 \cos \theta_2) \frac{dA_1 \cos \theta_1}{r_{12}^2}, \quad (1)$$

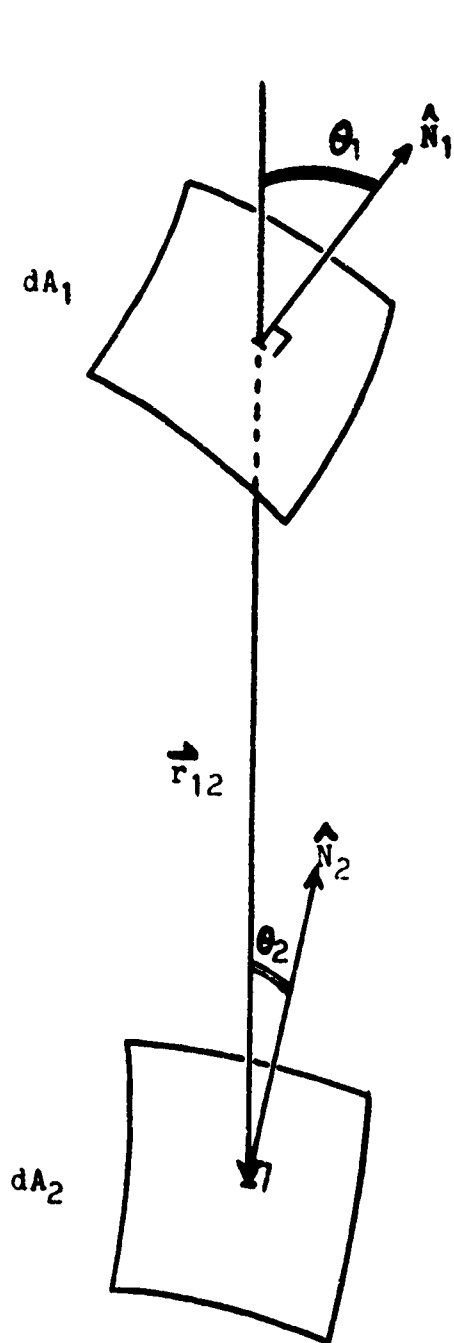


Figure 10. Variables in the through-particle problem.

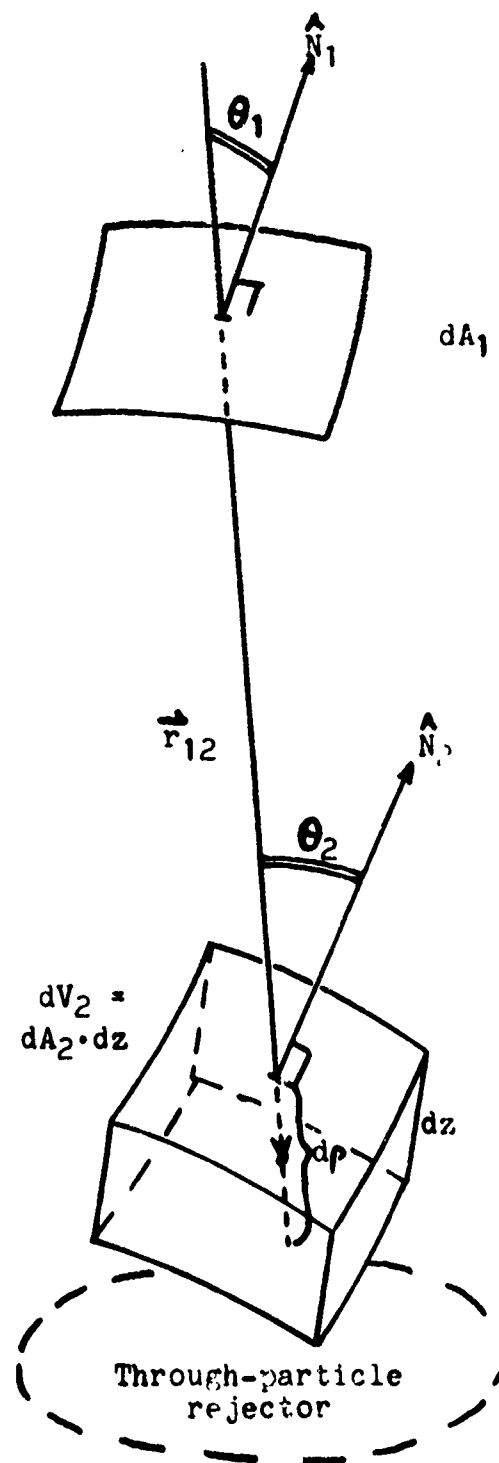


Figure 11. Variables in the stopping-particle problem.

where ϵ_1 and ϵ_2 are the detection efficiencies of dA_1 and dA_2 , which shall be assumed to be unity for the present. I is the intensity of penetrating radiation in the direction \vec{r}_{12} . I normally has the units

$$\frac{\text{particles}}{\text{cm}^2 \cdot \text{sr} \cdot \text{sec}} .$$

The term $\frac{dA_1 \cos \theta_1}{r_{12}^2}$ is just the solid angle $d\Omega$ determined by dA_1 and

\vec{r}_{12} . Thus, the exact count rate of a two-detector system is given by

$$R = \iint I(\vec{r}) dA \, \phi \Omega , \quad (2)$$

where $I(\vec{r})$ is the intensity function of incoming particles, A is the area of one detector, and Ω is the solid angle the second detector subtends.

The counted rate of stopping particles, however, is influenced by the energy spectrum of the incoming particles as well as by the flux intensity. A given particle must remove all of its momentum via some process (in the case of a muon, by ionization) in order to stop, and thus must transit a given thickness of material. For an elemental detector area dA_1 and an elemental stopping thickness $dA_2 dz$, the stopping particle problem is diagrammed in Figure 11. Assuming 100% rejection of through particles, the stopping-particle count rate is

$$dR = I(dA_2 \cos \theta_2) \frac{dA_1 \cos \theta_1}{r_{12}^2} \sigma \, dp , \quad (3)$$

where $d_1 = \frac{dz}{\cos \theta_2}$, and d is the stopping power of the detector material, expressed as momentum loss per unit length. The intensity I is now the differential flux, expressed as

$$\frac{\text{particles}}{\text{cm}^2 \cdot \text{sr} \cdot \text{sec} \cdot \text{momentum unit}}$$

For the particular situation of counting stopping muons at sea level, the intensity I is a slowly-varying function of energy, and a value of I is selected which corresponds to the mean value of energy deposited by a stopping particle.

The count rate of a stopping-muon detector may thus be expressed as

$$R = \sigma \iiint I(\vec{r}, \vec{E}) dA \, d\Omega \, d\rho, \quad (4)$$

or, knowing the Cartesian form of the differentials, as

$$R = \sigma \iiint \iiint I(\vec{r}, \vec{E}) dx_2 dy_2 \cos \theta_2 \frac{dx_1 dy_1 \cos \theta_1}{r_{12}^2} \frac{dz_2}{\cos \theta_2} \quad (5)$$

The terms $\cos \theta_2$ cancel, and the term r_{12} may be found if the area dA_1 and the volume $dA_2 dz$ are given Cartesian coordinates:

$$r_{12} = |\vec{r}_{12}| = \sqrt{(x_2 - x_1)^2 + (y_2 - y_1)^2 + (z_2 - z_1)^2}. \quad (6)$$

Additionally, $\cos \theta_1$ may be found if the orientation of dA_1 is known with respect to dA_2 . In this experiment, dA_1 is parallel to dA_2 for

the wide-angle muon telescope. (The x-y plane is chosen parallel to the plates and the stop tank's top face), making

$$\cos \theta_1 = \frac{z_1 - z_2}{r_{12}} . \quad (7)$$

For the zenith-angle detectors, conversely, due to their radial positioning, dA_1 is nearly perpendicular to \vec{r}_{12} for all positions, hence

$$\cos \theta_1 = 1.$$

The integration may now be performed as soon as the expression for $I(\vec{r})$ is specified.

Traditionally, the integral cosmic-ray distribution has been expressed as a power of the cosine of the zenith angle, that is, as

$$I(\theta, \phi) = I_0 \cos^n \theta , \quad (8)$$

where I_0 is the intensity of particles arriving vertically, and θ and ϕ are the zenith and azimuth angles of the particle's path.^(1,8,9) An exponent of zero corresponds to an isotropic flux, as is essentially the case with the primary radiation.⁽¹⁰⁾ At sea level, an exponent greater than zero is generated by attenuation through the greater atmospheric thickness traversed along larger zenith angles, and in the case of muons, by the greater decay probability along the longer paths of larger zenith angles.

A differential flux distribution $I(\theta, \phi, E)$ may be expressed as a

cosine-power law for any specific energy or energy band. The exponent n may vary from energy to energy within the measured range; however, as stated previously, the slowly-varying magnitude of the flux with energy, in the particles involved in this experiment, allowed the substitution of a single flux expression where the vertical flux value was averaged over the range of energies involved.

The approach of the cosine-power law was adopted in this experiment. The employment of this function has not always yielded a fit of high accuracy, but it does reflect its usage in the literature.

Employing the mean cosine-power expression for the flux, equation (5) becomes

$$R = \sigma I_0 \iiint \frac{(z_1 - z_2)^{n+1}}{r_{12}^{n+3}} dx_1 dy_1 dx_2 dy_2 dz_2 \quad (9)$$

for the case of parallel detectors, and hence for the wide-angle muon telescope. In the case of a zenith-angle detector, for which $\cos \theta_1 = 1$, equation (9) becomes

$$R = \sigma I_0 \iiint \frac{(z_1 - z_2)^n}{r^{n+2}} dx_1 dy_1 dx_2 dy_2 dz_2 \quad (10)$$

Appendix B contains a listing and a sample run of each of 3 BASIC-language programs designed to predict the zenith-angle detector coincidence rates using equation (10). For consistency, a grid spacing of 2" x 2" x 2" was used in all programs.

Program ZADRESP is predicated on the assumption that each zenith-

angle detector (hereafter called a ZAD) is sufficiently small that it may be treated as an elemental area; in terms of equation (5), dA_1 is equal to the entire ZAD scintillator area. For programs ZADRESP2 and ZADRESP3, the ZAD is divided into sixteen smaller dA_1 s. For the latter two programs, the coordinates of each dA_1 was first written into a file by the program ZADWRITE, from which file it was extracted in the course of the numerical integration.

The radial distance from the stop tank center to the ZADs being fixed at 63.0", the position of each ZAD may be specified by ζ and ξ , the spherical coordinates of its center relative to the stop tank center. These coordinates are different from θ and ϕ , the parameters of particle arrival path, since each ZAD counts particles with a range of directions. Figure 12 shows the variety of particle paths which a single ZAD counts, in coincidence with the wide-angle telescope.

Predictions made by program ZADRESP3 for various flux descriptions, i.e., for various values of the cosine-power n , are shown in Figure 13. The chi-square technique to be described in Section V compared these predictions to the actual data obtained from the ZADs. Assuming that an acceptable confidence level is obtained from the chi-square analysis, it is then valid to use the detector description of the ZADRESP programs in another program which predicts the response of the wide-angle telescope as a whole. Program MUPESP, in Appendix C, predicts the angular response for the wide-angle telescope, as well as the half-angle in the north-south and east-west planes. Its output is in units of $I_0 \sigma$, where σ is the scintillator stopping power. These results allow the comparison of the measured rate with the

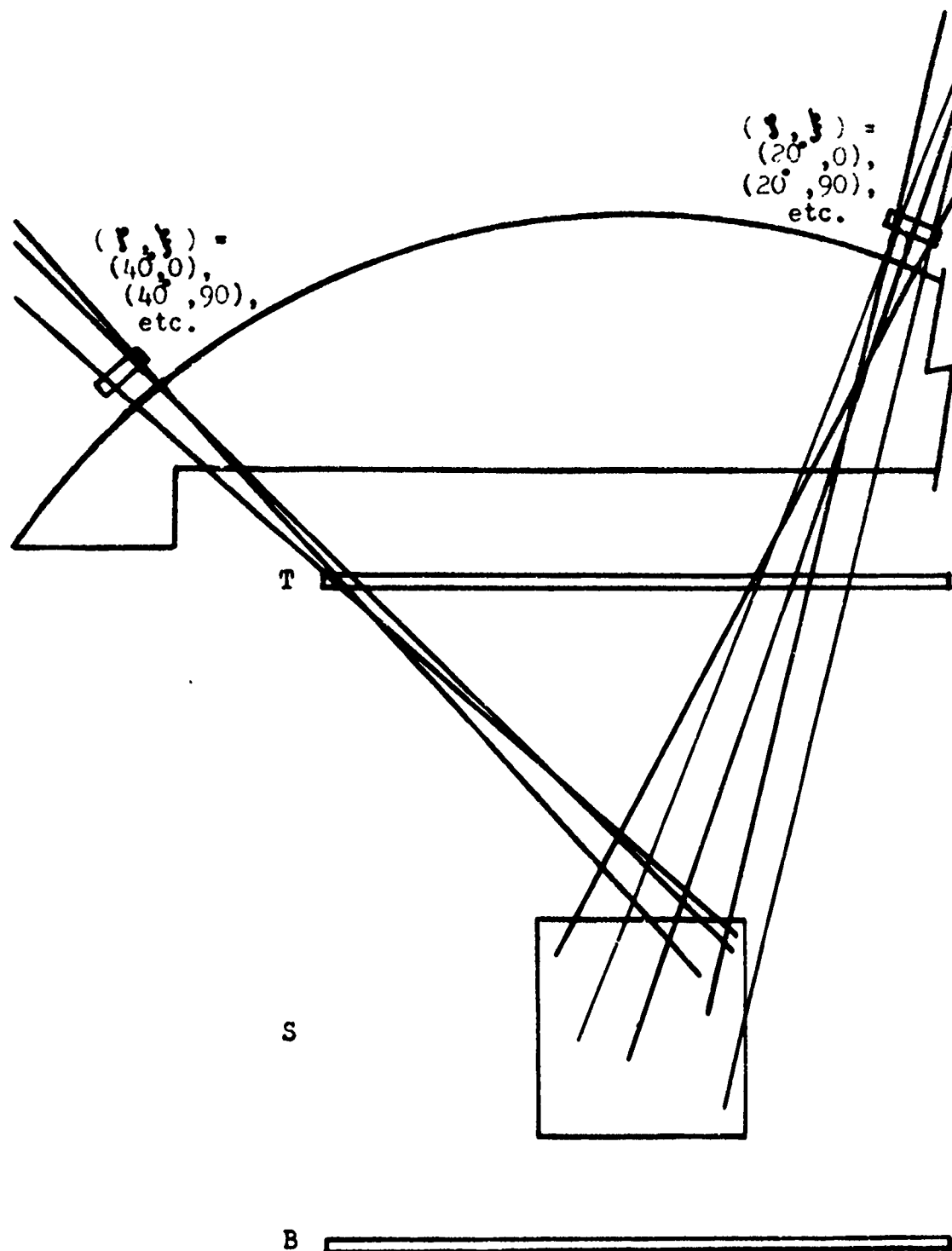


Figure 12. Variety of particle trajectories accepted by ZADs at $\theta = 20^\circ$ and 40° in the north-south or east-west planes.

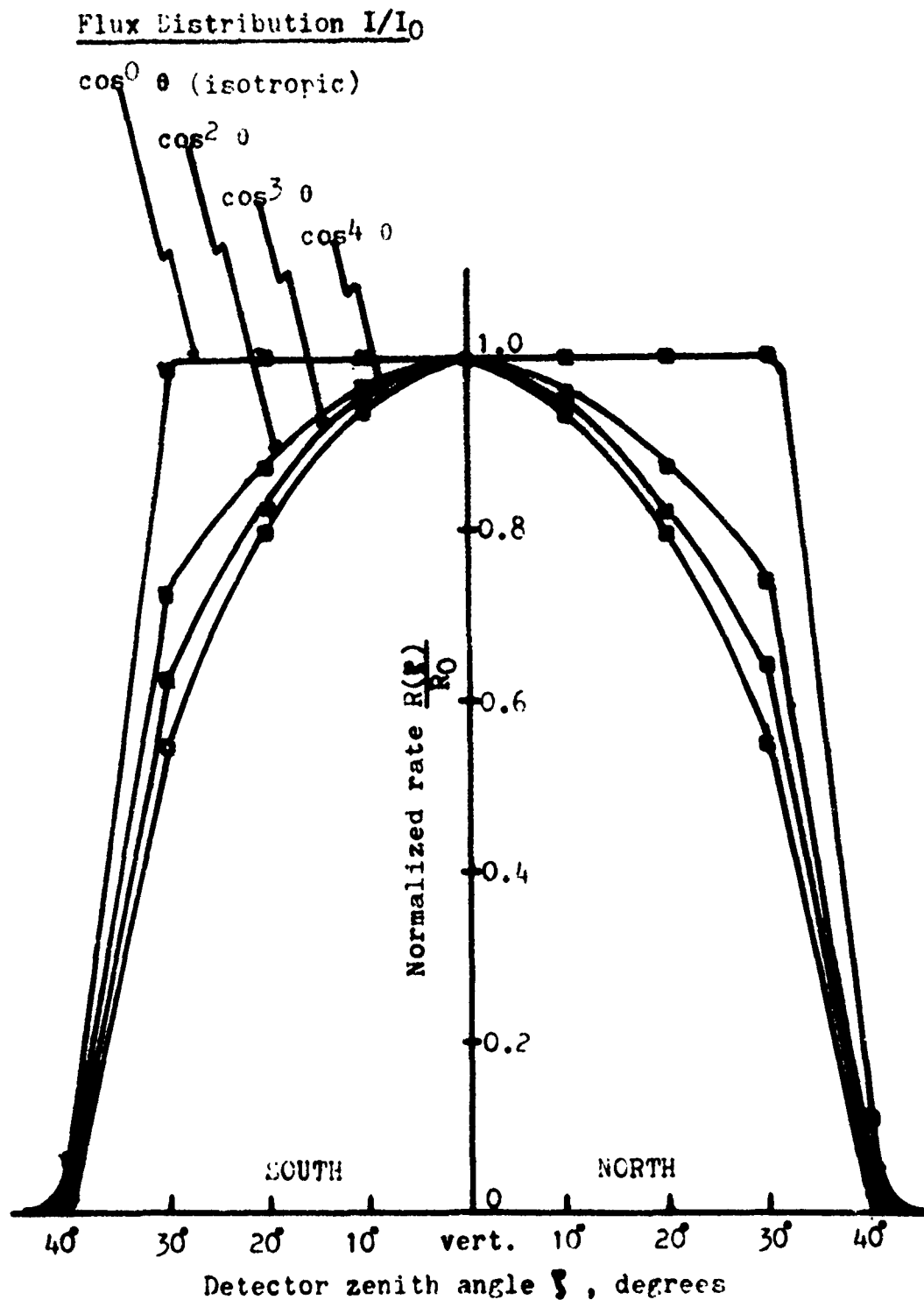


Figure 13. Normalized rates for ZADs in the north-south plane, for various flux descriptions, predicted by program ZADRESP3. [Note slight asymmetry due to stop tank offset from center of telescope.]

vertical flux measurements published by other authors, giving a value for detector efficiency of the stopping-muon system.

MURESP will, in addition, calculate the count rate expected within a given zenith-angle aperture. In this manner, the aperture within which half of the detected particles fall, the so-called half-angle, may be found directly. In the north-south plane, the half-angle indicates the expected influence of cosmic-ray sources to the north and south of the zenith circle on the celestial sphere. In the east-west plane, the half-angle indicates the expected time-width of an anisotropy in cosmic-ray rate, in either sidereal or solar time. Figure 14 shows the count rate as a function of zenith-angle aperture for various flux distributions. The half-angle, it may be seen, is a weakly-varying function of the flux cosine-power.

C. Detector Response by the Trajectory Method

Assume that a muon stopped at some point within the stop tank, and arrived along some path specified by θ and ϕ . One can determine whether or not the particle would have been counted according to whether the path passed inside or outside the boundaries of the top coincidence plate. Performing this operation for every point within the stop tank (or for the uniform matrix of points used in the ZADRESP programs) will yield the fraction of particles of each arrival direction (θ, ϕ) that are counted. If the results are summed in azimuth, the summation yields the relative ability of the muon telescope to count particles arriving from various zenith angles. This relative ability is, of course, independent of the flux distribution. The process was

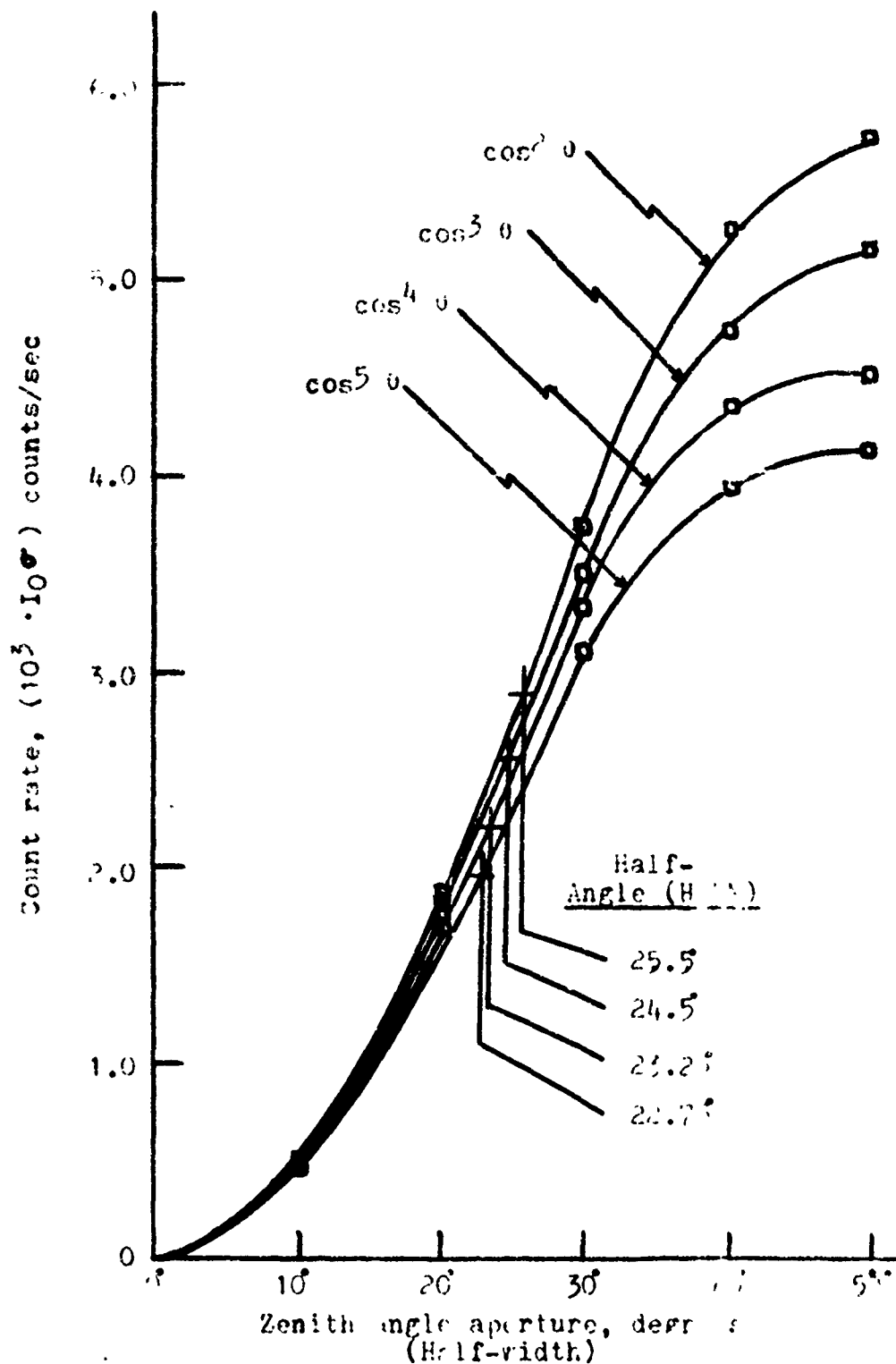


Figure 14. Number of counts seen by wide-angle photon telescope within various detection cones, as predicted by program MURPHY.

performed only for the wide-angle telescope and not for the zenith-angle detectors, due to the small solid angle that each ZAD subtends.

Program DETECTOR, listed in Appendix C, performs this process, assuming a symmetrical detector. Program DETECTOR2 uses more accurate detector dimensions, but yields the same zenith-angle response data. Figure 15 plots the relative counting rate of the wide-angle telescope as a function of particle zenith angle of arrival.

Multiplying the relative counting ability by the flux distribution for each angle, then multiplying again by the zenith-angle sine curve, yields the same aperture curve that program MURESP does. The DETECTOR programs are valuable because they isolate effects of the detector geometry from effects of the flux distribution.

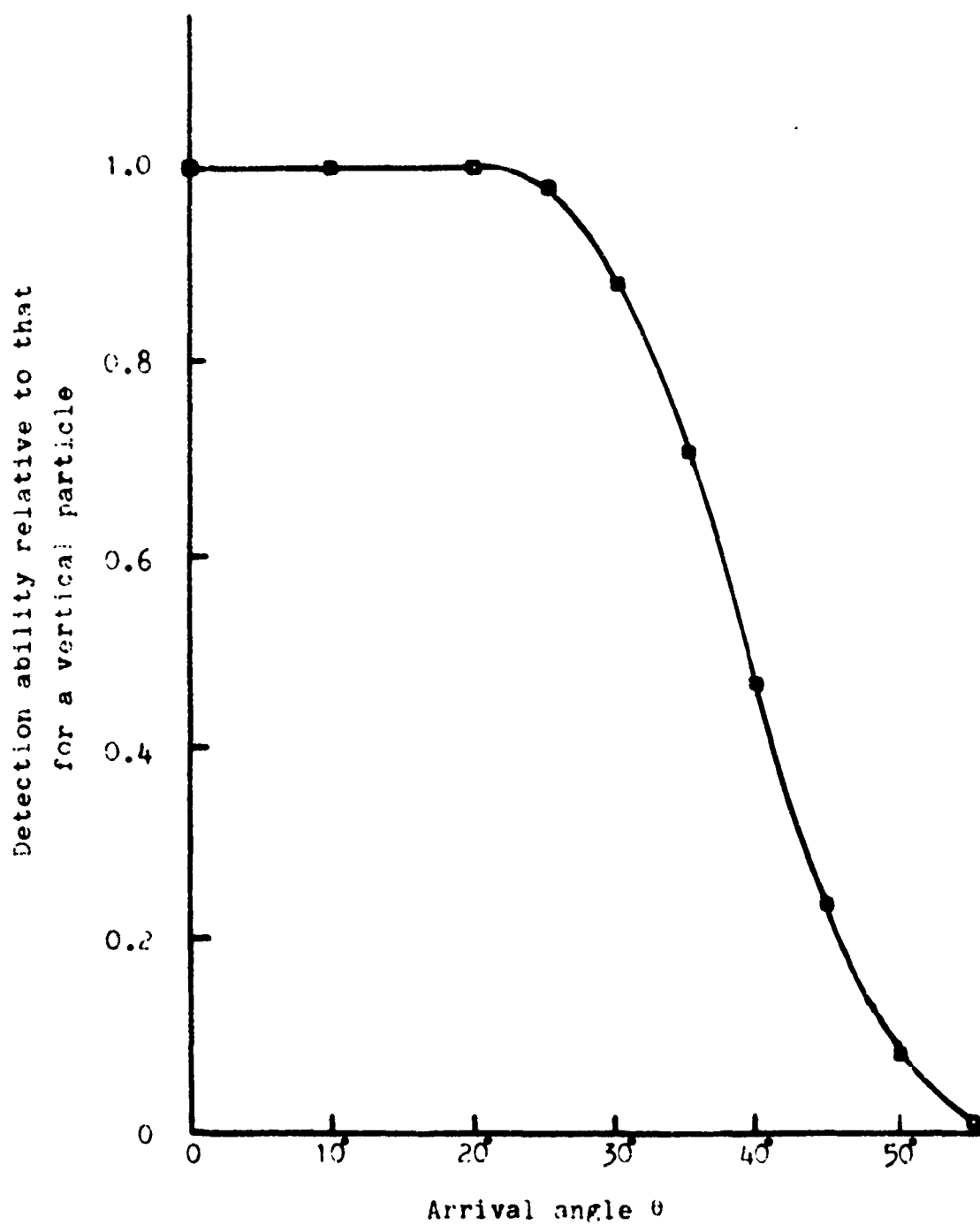


Figure 15. Relative detection ability of wide-angle telescope, generated by program DETECTR2.

IV. EXPERIMENTAL DETERMINATION OF ZENITH-ANGLE DISTRIBUTION

A. Collection of Data

Initially, a wide-angle muon rate of 800 counts per hour, and a ZAD solid angle of 0.5% of the total telescope solid angle, were assumed. A statistical accuracy of 5% was desired, requiring 400 counts, which should then have been available in 100 hours. To allow for variation, counts were made for one week in each ZAD configuration. Later, it was observed that the 100-hour figure was an under-estimate. The statistical error values will be stated along with the measurements.

For each count, due to limitations in the number of coincidence and discriminator units available, only three ZADs could be operated. Of the six ZADs available, three were chosen for their uniformity of response, and were not replaced during the course of the experiment. These ZADs were numbered 4, 9, and 15. ZAD number 4 was optically recoupled once during the course of the experiment, but neither its gain nor its response were affected.

Taking of data commenced on 22 October 1974, and was completed on 28 April 1975, with data being retrieved approximately weekly from the automatic data output system. No data was taken during the periods 17-26 December and 14-25 January. All data was in the form of typed and paper tape teletype outputs.

Normalized count rates were used rather than absolute rates in the data analysis. Normalization was done relative to the ZAD rate in the vertical position; thus, for each weekly count, one of the three ZADs was required to be in the vertical slot. Normalized

rates were used for the following reasons:

-- cosmic rays, especially low-energy ones, are susceptible to varying attenuation with atmospheric temperature and pressure variation; assuming that these variations would affect the flux equally at all angles, the normalization could eliminate pressure- and temperature-linked variations;

-- the flux description $I = I_0 \cos^n \theta$ is suited to a normalized description, since normalization eliminates dependence on the exact value of I_0 ; and

-- gain variations between tubes could be compensated for in normalizing, but not for absolute count rates.

Section B describes the compensation for ZAD efficiency, and Section C describes the calculation of statistical error. The sections following Section C explain the experimentally-determined corrections for various errors.

B. Detection Efficiency of Zenith-Angle Detectors

It was initially assumed that each ZAD was so constructed that its efficiency was, if not 100%, very nearly equal to that of each other ZAD. Preliminary examination of the data, however, showed the inaccuracy of this assumption. The method of reciprocity was applied to compensate for the differing efficiencies.

Consider a zenith-angle detector A, which has the position (ζ, ξ) , and a second detector B, in the vertical position. The rate counted by each detector is equal to the true rate (that

determined by detector geometry alone) multiplied by the efficiencies of each detector component; that is,

$$R_A(\zeta, \xi) = \epsilon_A \epsilon_T \epsilon_S R(\zeta, \xi) \quad (11)$$

and

$$R_B(0) = \epsilon_B \epsilon_T \epsilon_S R_0 \quad (12)$$

where $R(\zeta)$ and R_0 are the true muon rates through the angled and vertical positions, respectively. Assuming that the top plate and stop tank efficiencies are independent of zenith angle (see Section IV F), the apparent normalized rate becomes

$$\frac{R_A(\zeta, \xi)}{R_B(0)} = \frac{\epsilon_A}{\epsilon_B} \frac{R(\zeta, \xi)}{R_0} \quad (13)$$

Suppose that these detectors are now reversed, and a second count is taken, with B at (ζ, ξ) , and A at the vertical. This apparent normalized rate is then

$$\frac{R_B(\zeta, \xi)}{R_A(0)} = \frac{\epsilon_B}{\epsilon_A} \frac{R(\zeta, \xi)}{R_0} \quad (14)$$

Taking the product of the apparent normalized rates, the efficiencies cancel, and

$$\frac{R(\zeta, \xi)}{R_0} = \sqrt{\frac{R_A(\zeta, \xi)}{R_B(0)} \times \frac{R_B(\zeta, \xi)}{R_A(0)}} \quad (15)$$

Thus, the efficiency difference may be compensated for without knowing the individual efficiencies, by taking two counts with two detectors in reversed locations. The quantity $\frac{R(\zeta, \xi)}{R_0}$ will be referred to as a reciprocity-normalized count rate.

Table 4 lists the reciprocity-normalized rates for all of the mount positions at which measurements were taken. The second column contains the raw number of counts in each detector, the vertical count being the bottom number in each case. Each ratio was conducted with the same set of tubes as its reciprocal, that is, tubes 4 and 9, 9 and 15, or 15 and 4, with the exception of the data at $(\zeta, \xi) = 20^\circ$ north, where all three tubes were used, and reciprocity was obtained at that point with the relation

$$\frac{R(20^\circ N)}{R_0} = \left[\frac{R_9(20)}{R_4(0)} \times \frac{R_{15}(20)}{R_9(0)} \times \frac{R_4(20)}{R_{15}(0)} \right]^{1/3} \quad (16)$$

The third column of the table contains the reciprocity-normalized rates.

C. Statistical Error Calculation

The arrival times of cosmic ray particles may generally be treated as random occurrences. If a rate is indeed generated by randomly-distributed counts, the standard deviation of a number of counts may be conservatively estimated as the square root of that number; that is,

$$R(\zeta, \xi) = \frac{N \pm \sqrt{N}}{\Delta T} \quad (17)$$

A measured normalized rate may be expressed as

$$\frac{R(\xi, \xi)}{R(0)} = \frac{A \pm \sqrt{A}}{B \pm \sqrt{B}}, \quad (18)$$

where A and B counts are obtained by two detectors in the same time period. If this fraction is expanded, the deviation generated is probably somewhat larger than the standard deviation, a result of the propagation of errors. The expansion is

$$\begin{aligned} \frac{A \pm \sqrt{A}}{B \pm \sqrt{B}} &= (A \pm \sqrt{A}) \frac{1}{B} (1 \pm \frac{\sqrt{B}}{B})^{-1} \\ &\approx (\frac{A}{B} \pm \frac{\sqrt{A}}{B}) (1 \mp \frac{\sqrt{B}}{B}) \\ &\approx \frac{A}{B} (1 \pm \frac{\sqrt{A}}{A} \mp \frac{\sqrt{B}}{B}), \end{aligned} \quad (19)$$

where second-order terms have been dropped. A conservative statement of the standard deviation of a normalized rate is then

$$\sigma_N = \frac{A}{B} (\frac{1}{\sqrt{A}} \pm \frac{1}{\sqrt{B}}). \quad (20)$$

For a reciprocity-normalized rate, given that A and C are the numbers of particles counted at a particular mount position, and B and D are the vertical counts for the corresponding time interval,

the randomness error gives

$$\begin{aligned} \frac{R(\xi, \xi)}{R(0)} &= \sqrt{\frac{A}{B} \left(1 \pm \frac{1}{\sqrt{A}} \pm \frac{1}{\sqrt{B}}\right)} \sqrt{\frac{C}{D} \left(1 \pm \frac{1}{\sqrt{C}} \pm \frac{1}{\sqrt{D}}\right)} \\ &= \sqrt{\frac{AC}{BD}} \sqrt{1 \pm \frac{1}{\sqrt{A}} \pm \frac{1}{\sqrt{B}} \pm \frac{1}{\sqrt{C}} \pm \frac{1}{\sqrt{D}}} , \end{aligned} \quad (21)$$

again neglecting second-order terms. An exaggerated estimate of one standard deviation is given when all error terms in equation (21) are either positive or negative, i.e.,

$$\sigma_{RN} \pm \sqrt{\frac{AC}{BD}} \left[\sqrt{1 \pm \frac{1}{\sqrt{A}} \pm \frac{1}{\sqrt{B}} \pm \frac{1}{\sqrt{C}} \pm \frac{1}{\sqrt{D}}} - 1 \right] . \quad (22)$$

This is actually the unbiased estimate of σ_{RN} , rather than the σ_{RN} generated by data distribution. The last column of Table 4 contains the σ_{RN} for each data point.

All mathematical eliminations and error predictions have now been performed. Experimental determination of certain systematic errors is explained in the following sections.

D. Shower Corrections

Often, following a primary particle's interaction with an atmospheric nucleus, the reaction products have sufficient energy to cause further nuclear interactions. The propagation of such a shower of secondary cosmic rays is such that many particles may

arrive at the earth's surface simultaneously. Should a stopping muon be associated with other particles in a shower, a zenith-angle detector may be erroneously triggered by an associated particle, the resulting event signature mimicking that of a muon passing through the ZAD. Figure 16 demonstrates the generation of a shower-produced count.

Because the arrival directions of showers are strongly concentrated about the vertical, ZADs at mount positions nearer the vertical were not expected to accrue shower-generated counts, since many of the associated particles should pass through the bottom anti-coincidence plate, negating the entire event. Detectors with $\tau = 40^\circ$ in any plane, and with $\tau = 30^\circ$ in the north-south and east-west planes, however, did not project onto the bottom plate, and were thus deemed to be susceptible to shower-generated counts.

A means of correcting the data from these points was created by mounting a detector vertically beneath the scintillator of a 30° or 40° detector. In this position, shown in Figure 17, the lower detector is susceptible to approximately the same number of shower-generated counts as the ZAD above it; however, because it is mounted below the plane of the top coincidence plate, it can register no true counts. The reciprocity-normalized rates of these shower detectors were applied as negative corrections to the corresponding ZAD rates. The shower correction was found to be $(-.024 \pm .006)R_0$ at $\tau = 40^\circ$, and $(-.064 \pm .01)R_0$ at $\tau = 30^\circ$.

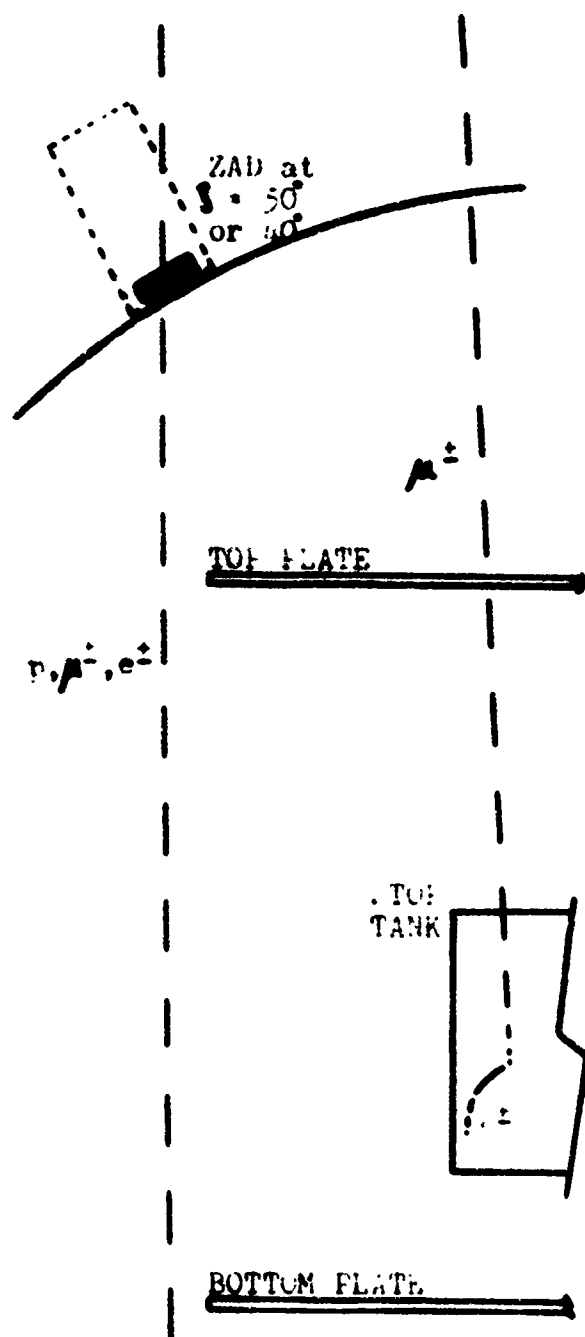


Figure 16. Shower-generated
ZAD count (not to scale.)

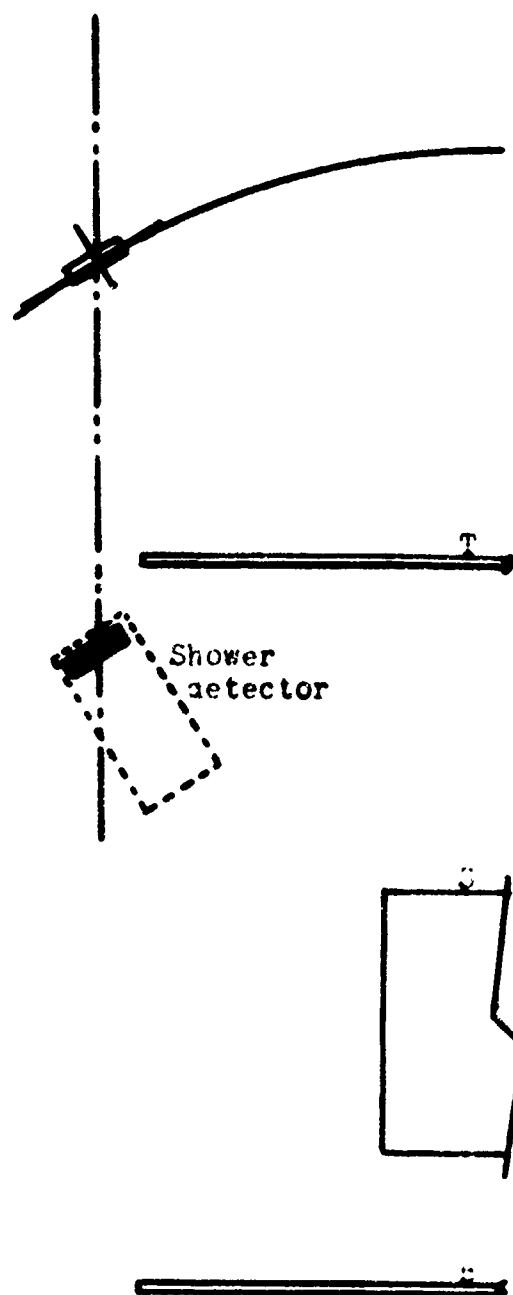


Figure 17. Location of detector for experimental determination of shower correction, $\theta = 30^\circ$ (not to scale.)

E. Correlated-Pulsing Corrections

Due to the geometry of the wide-angle muon telescope, it is possible for some through particle trajectories to trigger a $TS\bar{B}$ count by missing the bottom plate, as shown in Figure 18. Further, some of these trajectories may intersect the boundaries of a ZAD in the $(\zeta, \xi) = 40^\circ$ north, east, south, and west positions. Should any S pulse be generated in the acceptance interval thereafter, that is, between 0.3 and 5.3 μ sec later, an erroneous count will be generated. The $S\bar{T}\bar{B}$ pulses following a false $TS\bar{B}$ count may come either from the random impact of cosmic rays, from random noise, or from a correlated second pulse generated within the system.

A multichannel analyzer accumulation of the "stopping-muon" decay times was available for all data taken between 22 October 1974, the beginning of this experiment, and 1 February 1975. Comparison of this time-domain data with the theoretical muon decay curve indicated that approximately 20% of all muon counts accumulated to that time were generated by either correlated pulsing or accidental coincidences. To test the possibility that accidental coincidences were responsible, the $TS\bar{B}$ and $S\bar{T}\bar{B}$ rates were measured, and the accidental rate was calculated. The results were:

$$R_{TS\bar{B}} = 175 \frac{\text{counts}}{\text{min}} = 2.92 \text{ cps}$$

$$R_{S\bar{T}\bar{B}} = 2100 \frac{\text{counts}}{\text{min}} = 35 \text{ cps}$$

$$\begin{aligned} T_Y &= \text{decay pulse acceptance window} \\ &= 5.0 \times 10^{-6} \text{ sec} \end{aligned}$$

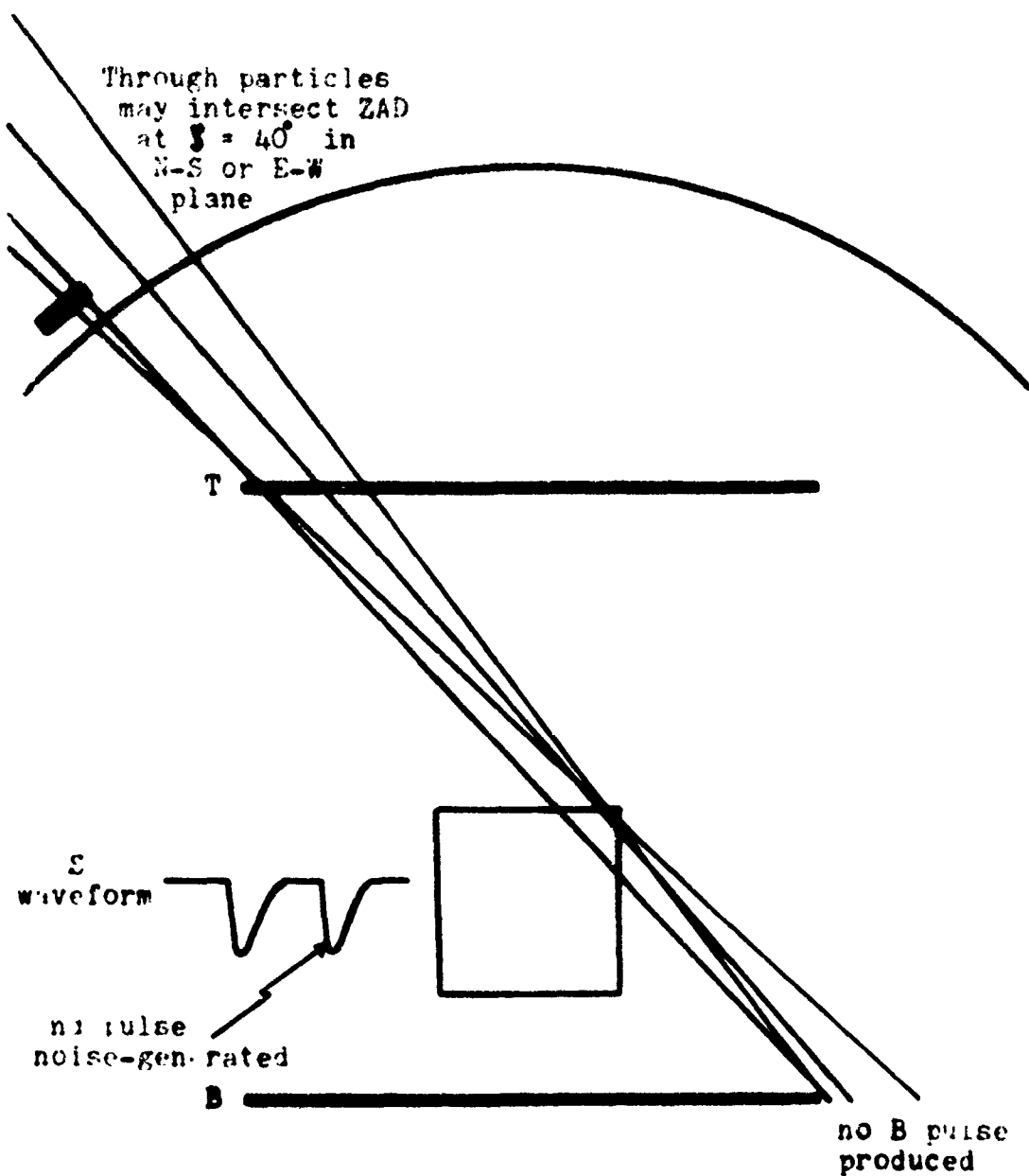


Figure 18. Generation of TSB pulses by through particles, leading to acceptance of false muon signatures.

These figures yield an accidental rate of 5.11×10^{-4} cps. The raw muon rate at that time was approximately 900 $\frac{\text{counts}}{\text{hour}}$, or .25 cps, indicating that the 20% excess in counts could not have been generated by purely random coincidences.

At least one known phenomenon can explain second pulses in the stop tank that are coupled to those produced by cosmic rays. Should a gas, such as air, leak into one or both of the 5" photomultiplier tubes, its ionization by the accelerated photoelectrons from a scintillator flash would make it a charge carrier. Sufficient quantities of such charged particles dislodging more electrons from the photo-cathode could cause one or many correlated pulses.

Correlated pulsing was observed on an oscilloscope when the 5" tubes were decoupled from the stop tank and triggered by a pulsed light source. The correlated pulsing was at all times less than 150 millivolts in amplitude, and was concentrated about a 0.8 μsec lag behind the initiating pulse. This lag corresponded to a prominent peak in the time-domain spectrum.

Approximately 80% of the correlated pulsing was eliminated upon reducing the 5" phototube voltage from 2300v to 2200v. After recoupling the 5" tubes to the stop tank, the correlated pulsing was further reduced by increasing the stop tank discriminator thresholds from 20 mv to 100 mv. A variety of discriminator thresholds was examined, 100 mv being the lowest possible setting which coincidences between through cosmic rays (TBS) and stop tank second pulses (STB).

Following this correction, the average stopping muon count rate decreased from about 900 counts per hour to about 540 counts per hour. This 40% decrease was somewhat greater than the drop expected from the elimination of correlated-pulse counts, implying that the detection efficiency of the system had decreased. However, the time-domain data now showed no noise-generated peaks or other anomalies, and the half-life obtained from it was within 2% of the published muon half-life in organic compounds.⁽¹¹⁾

However, a time-domain accumulation of "muons" detected by the 40° S detector only showed that approximately 20% of these counts were still caused by multiple pulsing. This is not inconsistent with a correlated-pulsing rate of 0.3% or less from the wide-angle telescope as a whole. The requirement was set that no data from the 40° N or 40° S positions be accepted from the time period before the reduction of the stop tank tube gain. To the accepted data was applied a correction of $(-.20 \pm .05)R_{40N,S}$, or $(-.020 \pm .005)R_0$.

F. Compensation for Counting Efficiency of Muon Telescope Components

As has been shown in Section IV A, the detection efficiency of the zenith angle detectors can be corrected for by switching two detectors between an angled position and the vertical. However, no such simple means exists for correcting for variations in efficiency within the large components of the muon telescope, although these efficiency variations are measureable.

The efficiencies at various positions on the top and bottom plates

were measured by the "sandwich" method, using the detectors described in Section II C. Figure 19 is a schematic representation of two small detectors being used to measure a local efficiency of a larger planar detector P. Sn_1 and Sn_2 represent the smaller "sandwich" detectors. The count rate of Sn_1 and Sn_2 in coincidence is

$$R_{12} = \epsilon_1 \epsilon_2 G I_0 , \quad (23)$$

where ϵ_1 and ϵ_2 are the sandwich detector efficiencies, G is a geometrical factor due to the areas and arrangement of Sn_1 and Sn_2 , and I_0 is the vertical flux. It can be seen from the figure that every particle that passes through both Sn_1 and Sn_2 must also pass through P; the count rate of Sn_1 , P, and Sn_2 in coincidence is then given by

$$R_{1P2} = \epsilon_1 \epsilon_P \epsilon_2 G I_0 ; \quad (24)$$

therefore,

$$\epsilon_P = \frac{R_{1P2}}{R_{12}} . \quad (25)$$

Measurements of this sort were conducted in various regions of the top and bottom plates, and the results are recorded in Figures 20 and 21. These measured efficiencies are accurate to $\pm 10\%$.

Figure 20 indicates that the corner areas of the top plate are significantly less than 100% efficient. Particles detected by ZADs in the 40° NE and 40° SE positions must pass through these regions

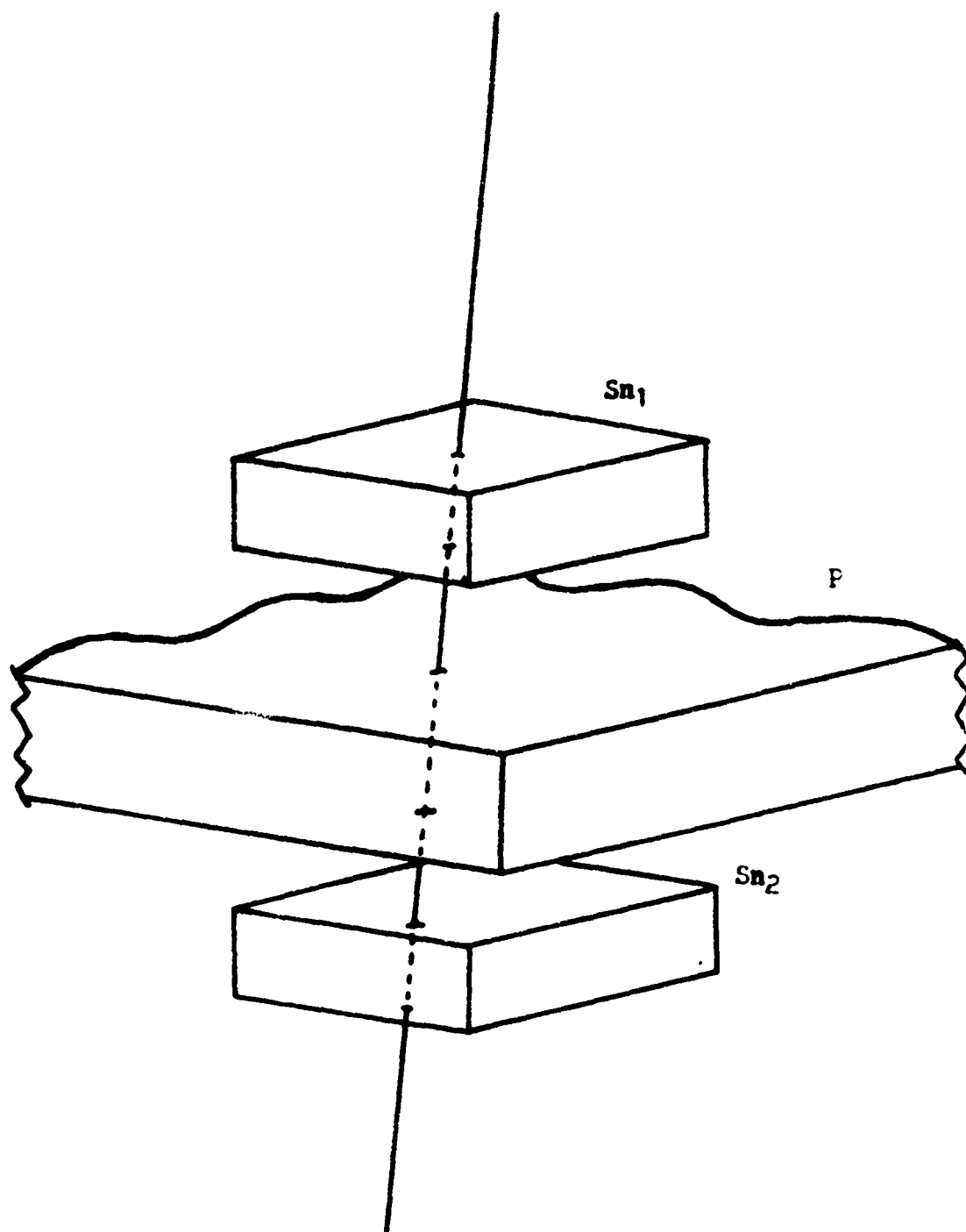


Figure 19. Measurement of the efficiency of a planar detector by means of the "sandwich" method. All particles passing through both Sn_1 and Sn_2 are constrained to pass through P as well.

Figure 20.
Top plate.

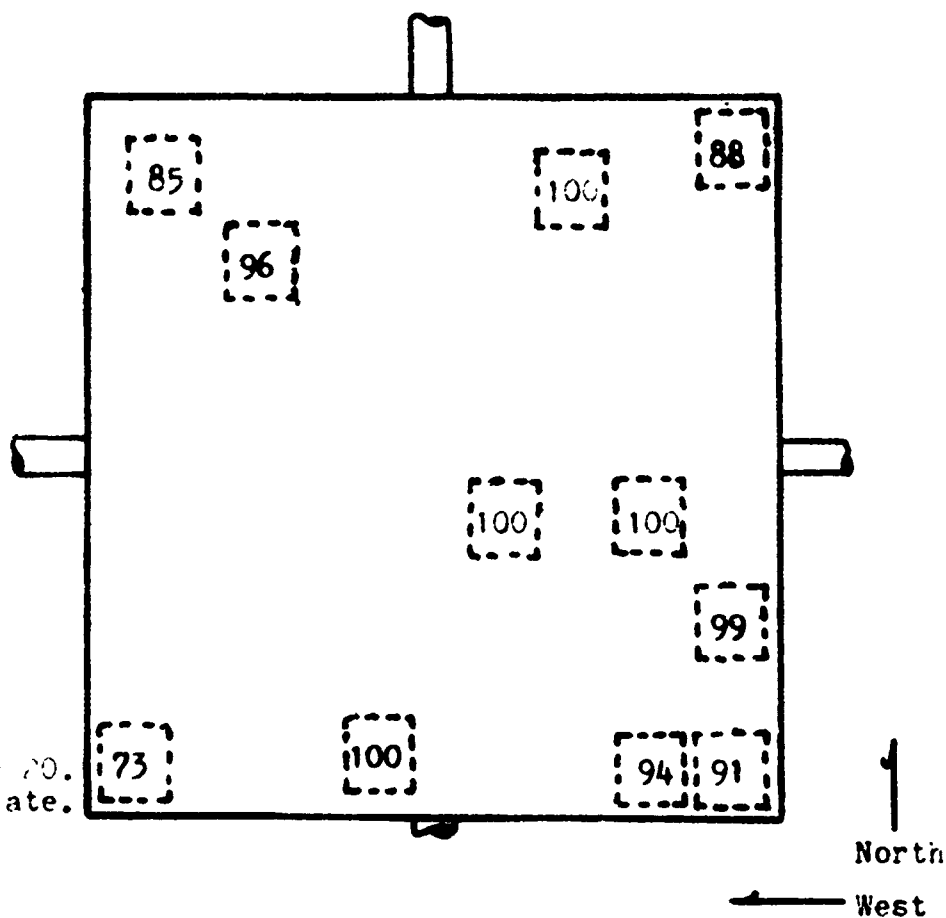
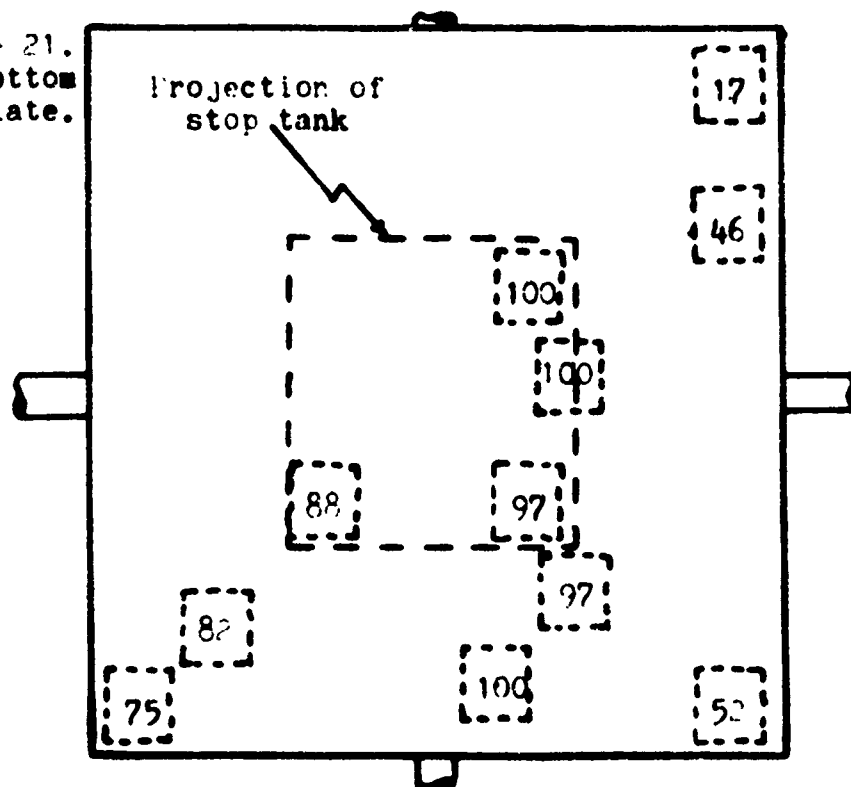


Figure 21.
Bottom plate.



Figures 20 and 21. Efficiency measurements of top and bottom plates, respectively, by "sandwich" method. Dotted areas of local efficiencies are drawn to scale.

enroute to the stop tank. Thus the apparent rates seen by ZADs in these positions are lower than the true rates. The exact amount of enhancement required is uncertain, but is probably between zero and 15%. The correction due to low corner efficiency was, then, $(+.08 \pm .08)R_{40NE,SE}$, or $(+.021 \pm .021)R_0$.

It is also apparent, from Figure 21, that the low efficiency regions of the bottom plate allow some false PSB counts to be generated. The correction for this effect is inherent in the correlated pulsing corrections to the 40° N and 40° S positions (see Section IV E), and no additional correction is required.

Because of the difficulty of measuring local efficiencies within the stop tank, and because the small stop tank volume was viewed by two high-efficiency, high-gain photomultiplier tubes, the stop tank counting efficiency was assumed to be 100% throughout the course of the experiment.

G. Positional Error of Zenith-Angle Detectors

It was felt that the position of each ZAD was known to $\pm 0.5''$ in any direction. This error is insignificant for all except the 40° N and 40° S locations; as may be seen in Figure 13, a small change in the real position of a 40° N or 40° S detector causes a large fractional change in count rate. Accordingly, after all other corrections were made to these points, R_{40N} and R_{40S} were scaled up by a factor of 2.5, due to rate variations with position.

V. COMPARISON OF MEASURED DATA AND PREDICTED RESPONSE

A. The Chi-Square Fit

A standard method of determining which of several theoretical expressions best fits a set of experimental data is the "chi-squared test." In this process, the quantity

$$S = \sum_{i=1}^k \frac{(Q_i - N_i)^2}{N_i} \quad (26)$$

is to be minimized, where the Q_i are observed data points, and the N_i are the corresponding theoretical values, selected from any of several predictions. In addition to yielding the best-fitting theoretical curve, the process can measure, although subjectively, the goodness of fit of any theoretical curve. The number of points k , assuming that the Q_i are independent of one another, is known as the number of degrees of freedom.

The magnitude of S , as expressed in equation (26), is applicable only when the Q_i and N_i are total numbers of counts, whereas this experiment deals with normalized rates. To relate the two, assume that an observed rate R_i is equal to $\frac{Q_i}{T_i}$, and similarly that a theoretical rate P_i is equal to $\frac{N_i}{T_i}$. Then

$$S = \sum_{i=1}^k T_i \frac{(R_i - P_i)^2}{P_i} \quad (27)$$

For a normalized rate, R_i must be divided by the normalizing rate R_i^0 , and P_i by the theoretical rate P_i^0 , which cannot be expressed exactly

in terms of equation (27). An approximation may be made by dividing both the R_i and P_i by R_i^0 , which gives

$$S = \sum_{i=1}^k T_i R_i^0 \frac{\left(\frac{R_i}{R_i^0} - \frac{P_i}{R_i^0} \right)^2}{P_i / R_i^0} \quad (28)$$

The products $T_i R_i^0$ are simply the number of counts in the vertical detector over the time periods T_i . Equation (28) is also applicable to reciprocity-normalized rates, if the substitutions

$$\frac{R_i}{R_i^0} = \sqrt{\frac{A_i C_i}{B_i D_i}} \quad (29)$$

$$T_i R_i^0 = \sqrt{B_i D_i} \quad (30)$$

and

$$\frac{P_i}{R_i^0} = P_i' \quad (31)$$

are made, where the A_i and C_i are the raw numbers of ZAD events at (ξ_i, ξ_i) , and the B_i and D_i are the events in the vertical ZADs, for each time T_i . The P_i' are simply the predictions of normalized rates of a program such as ZADRESP3. S is now used in this form,

$$S = \sum_{i=1}^k \sqrt{B_i D_i} \frac{\left[\frac{R_i(\cdot)}{R_i(0)} - P_i' \right]^2}{P_i'} \quad (32)$$

in the program RESULTS, listed in Appendix D. This value of S is labeled "FLAT S" in the output of RESULTS, for reasons which will be apparent later.

The drawbacks of the formula for S developed in equations (26) through (32) are that it is an approximation, improperly normalized as of equation (28), and gives equal weight to each data point. Equation (26) is actually valid only when $N_i = \sigma_i^2$, i.e., when the Q_i are Gaussian-distributed about the N_i . Should some of the measured rates have large known systematic errors, S would become unreasonably large.

A more universally applicable expression for S is given by

$$S = \sum_{i=1}^k \frac{(Q_i - N_i)^2}{\sigma_i^2}, \quad (33)$$

where the σ_i are the standard deviations corresponding to the Q_i (after Wolberg.¹²) The reasons for preferring equation (33) may be stated briefly. Using this expression, the statistically poorer points receive less weight in the calculation of S. Further, any known errors which are systematic in nature, but which cannot be made an exact correction to the data (e.g., the low efficiency of the top plate corner regions), may be stated as an increase in the value of the uncertainty σ_i . Finally, equation (33) is not limited in its applicability to numbers of counts; rather, the Q_i and N_i may be used directly as normalized rates and reciprocity--normalized rates. Program RESULTS outputs the value of equation (33) as "WEIGHTED S".

The actual use of the variable χ^2 is as a reference; that is, values of χ^2 are tabulated, as a function of certain "confidence levels," the measure of goodness of fit mentioned earlier, and of k , the number of degrees of freedom. S is compared to these tabulated values.

B. Analysis of Data

Table 5 is a summary of all of the corrections in Section IV, along with the net results upon each normalized rate and σ . These were the corrections employed in program RESULTS, which performed the S-minimization process by evaluating S for various values of the cosine-power n . In Figure 22, the weighted S values generated by equation (33) are given for various values of the cosine-power. The upper curve was generated using uncorrected values for the reciprocity-normalized data points, and is shown for comparison only. The lower curve, when all corrections have been applied, clearly shows that S is minimized when the cosine-power is about 4.7. Further, published χ^2 tables^(12,p.67) may be used to find the relative probability that the data came from each set of predicted values. From these relative probabilities, the "confidence levels" described previously, it may be seen that n probably deviates from the value 4.7 by no more than ± 0.5 :

n	<u>weighted S</u>	<u>Relative Closeness of Fit</u>
3.5	25.5	<0.01
4	13.1	0.2
4.5	7.64	0.7
5	7.77	0.7
5.5	12.0	0.3

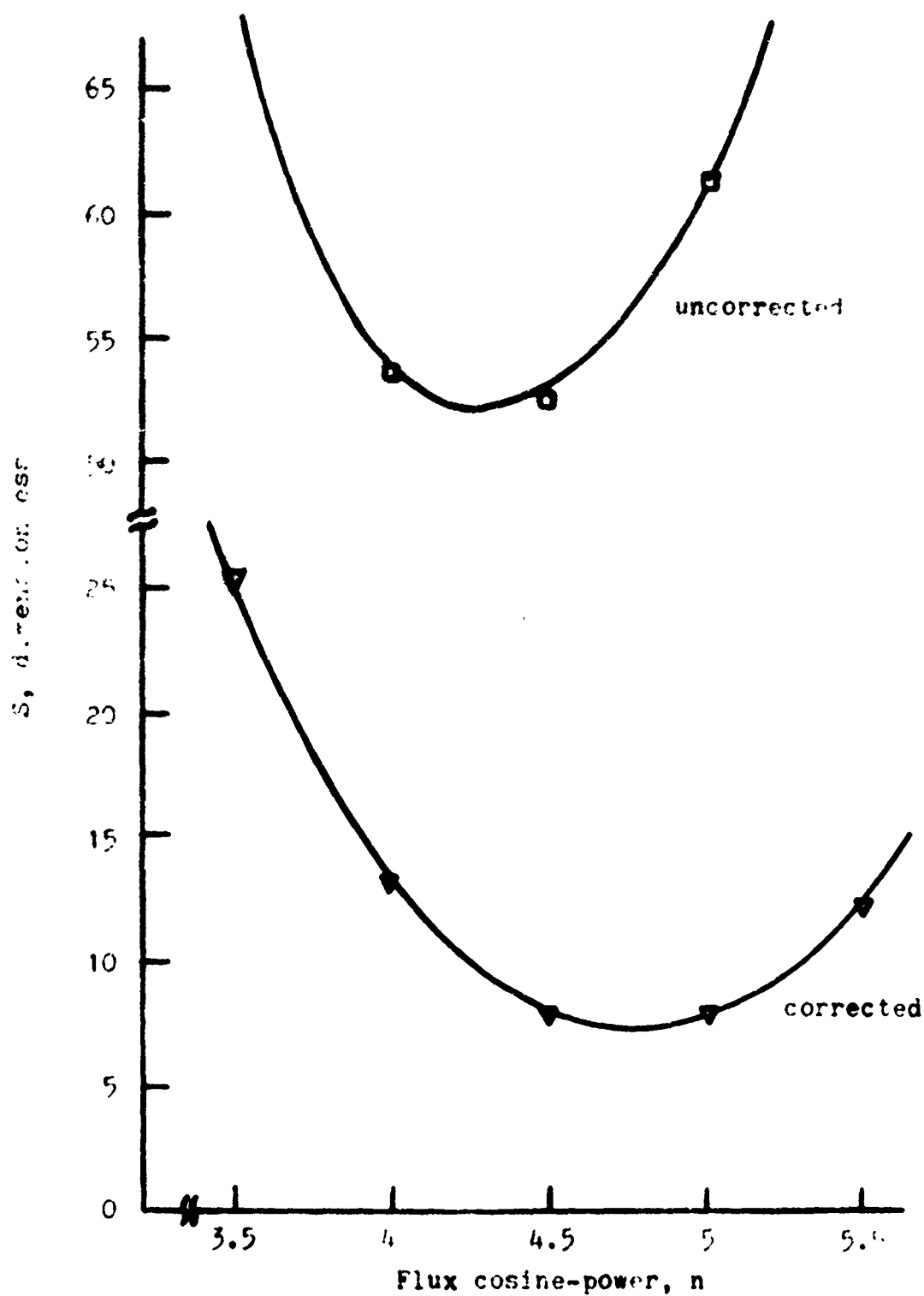


Figure 22. Weighted S curves for all data ($k = 10$ degrees of freedom), generated by uncorrected and corrected data. Computations by program RESULTS.

In order to show the influence of the marginal data points on the value of S , the curves in Figure 23 were generated by data excluding that at the marginal points 40° N and 40° S. Compare the dotted curve to the uncorrected 10-point curve at the top of the figure. The dotted curve, which excludes the marginal points but employs no other corrections, shows that the error in the uncorrected data is due mainly to the 40° N and 40° S data. Adding the corrections to the 8-point curve generates the solid curve which, it may be seen, is very similar to the 10-point curve in Figure 22.

The flat- S values generated by equation (32) are plotted in Figure 24. They were not employed in the data analysis, because equation (32) is not considered to weight the data points properly.

The confidence levels quoted in this section should not be interpreted as a measure of confidence of the observer. Rather, they represent a relative measure of the closeness of fit of each set of predicted to the measured data.

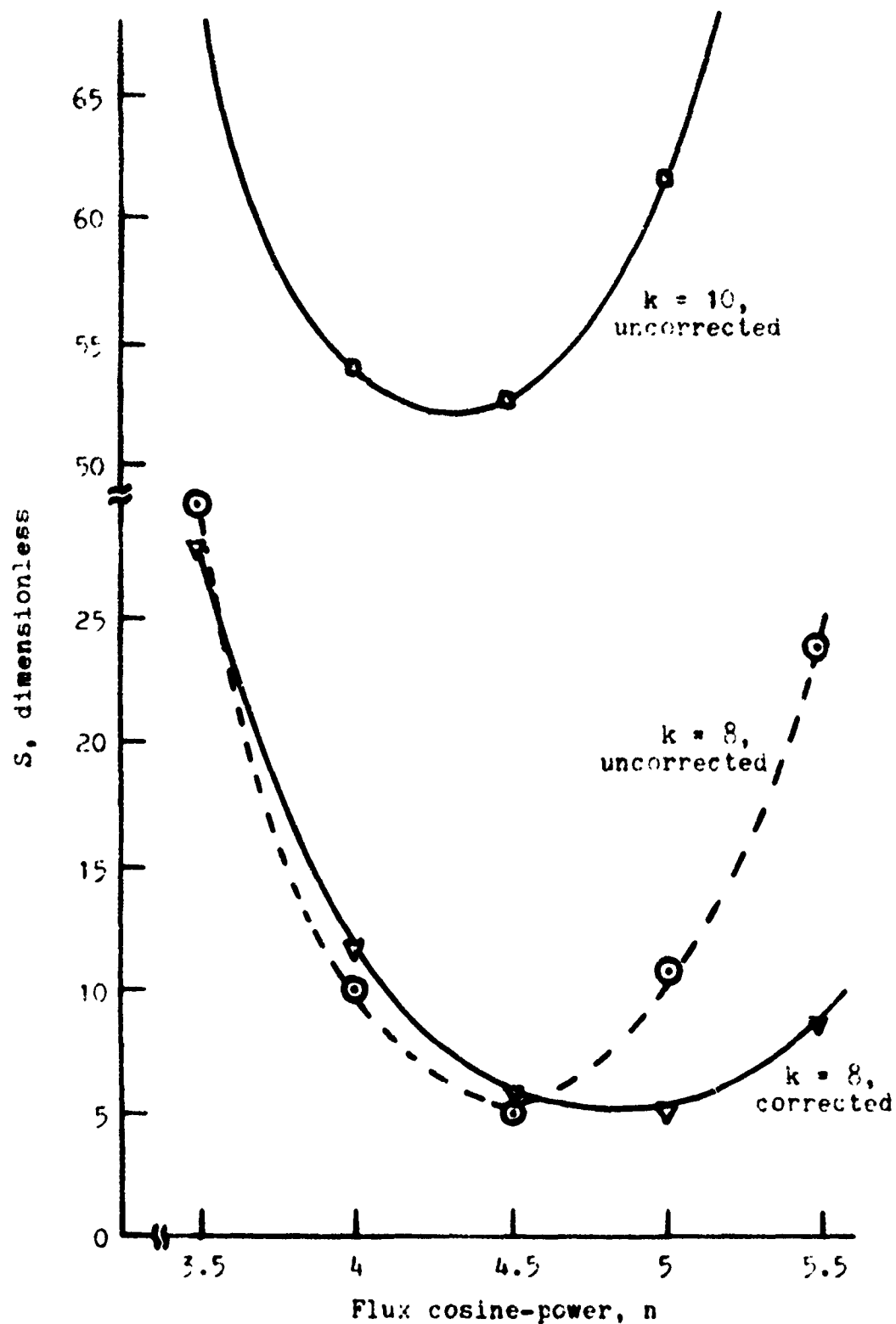


Figure 23. Comparison of S for data exclusive of 40° H and 40° S data ($k = 8$ degrees of freedom), with S curve generated by 10 uncorrected data points ($k = 10$). Computations by program RESULTS.

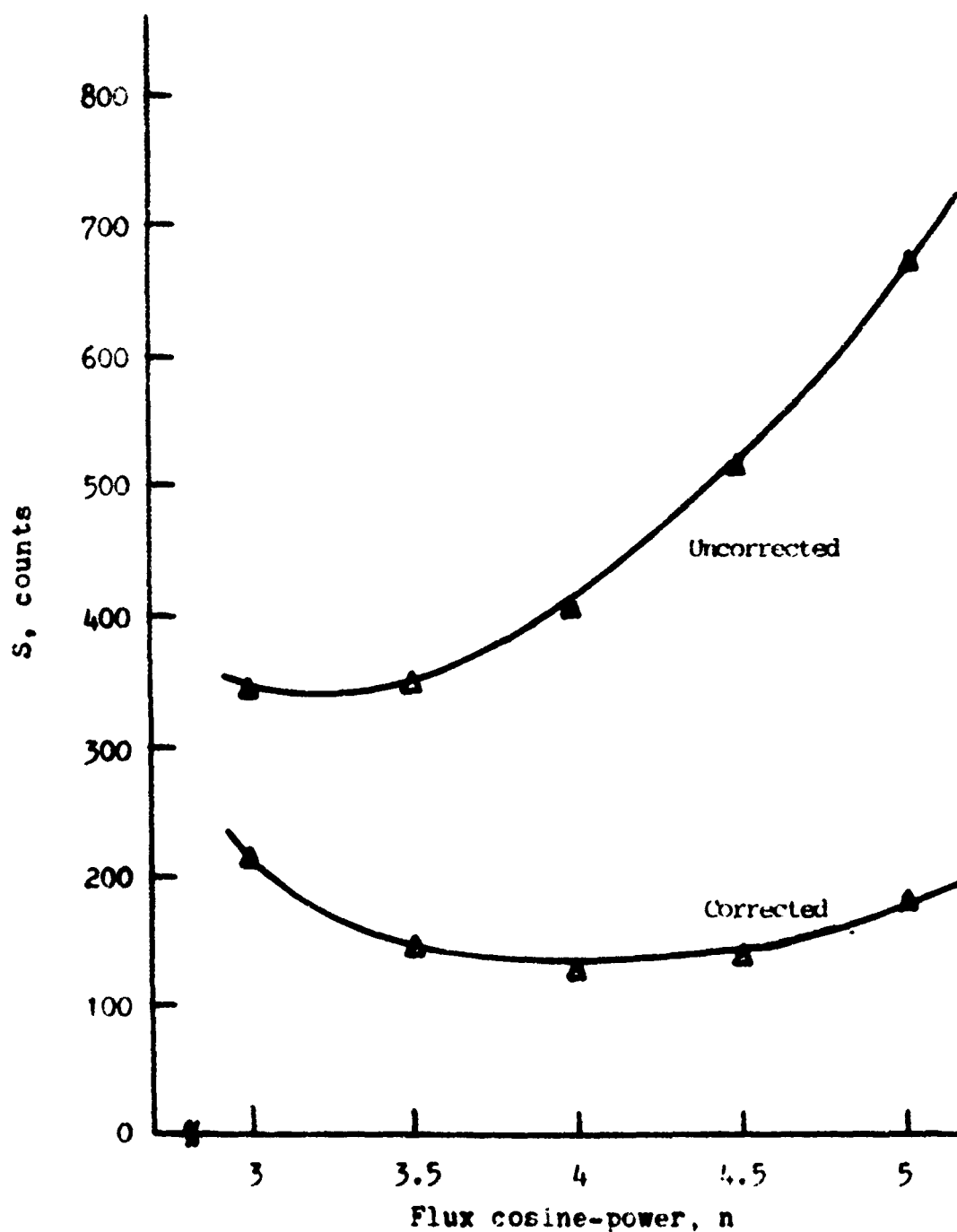


Figure 24. Flat (unweighted) S curves for all data ($k = 10$ degrees of freedom), generated by uncorrected and corrected data. Computations by program RESULTS.

VI. DISCUSSION OF RESULTS

A. Mathematical Description of Detector System

The program MURESP is an example of inductive logic --it springs from the description of the zenith-angle detection system in the ZADRESP programs. Its validity, therefore, depends upon two criteria of induction: the accuracy with which the ZADRESP programs predicted the response of the wide-angle telescope in coincidence with the zenith-angle detectors; and the validity of replacing the zenith-angle detectors with the top coincidence plate as a whole.

Figure 25 shows the corrected data in the north half-plane and at the 40° northeast position, superimposed upon the ZADRESP3-generated rate predictions for $n = 4.5$ and $n = 5$. The error bars are of the values computed by program RESULTS. All corrected data points are within one standard deviation of the predicted curve, indicating that ZADRESP3 indeed provides an accurate description of the ZAD-coupled wide-angle telescope response, satisfying the first criterion for induction.

It is assumed that the second criterion is satisfied, since the area elements of the top plate may be made arbitrarily small. The resulting detector description is then identical to that for a ZAD except for a factor of $\cos \theta$. The predictions of MURESP may then be said to be accurate within the limits of this experiment. These predictions are:

-- a wide-angle telescope half-angle (zenith-angle within which half of all particles are detected) of $23.0^\circ \pm .25^\circ$, or a full width

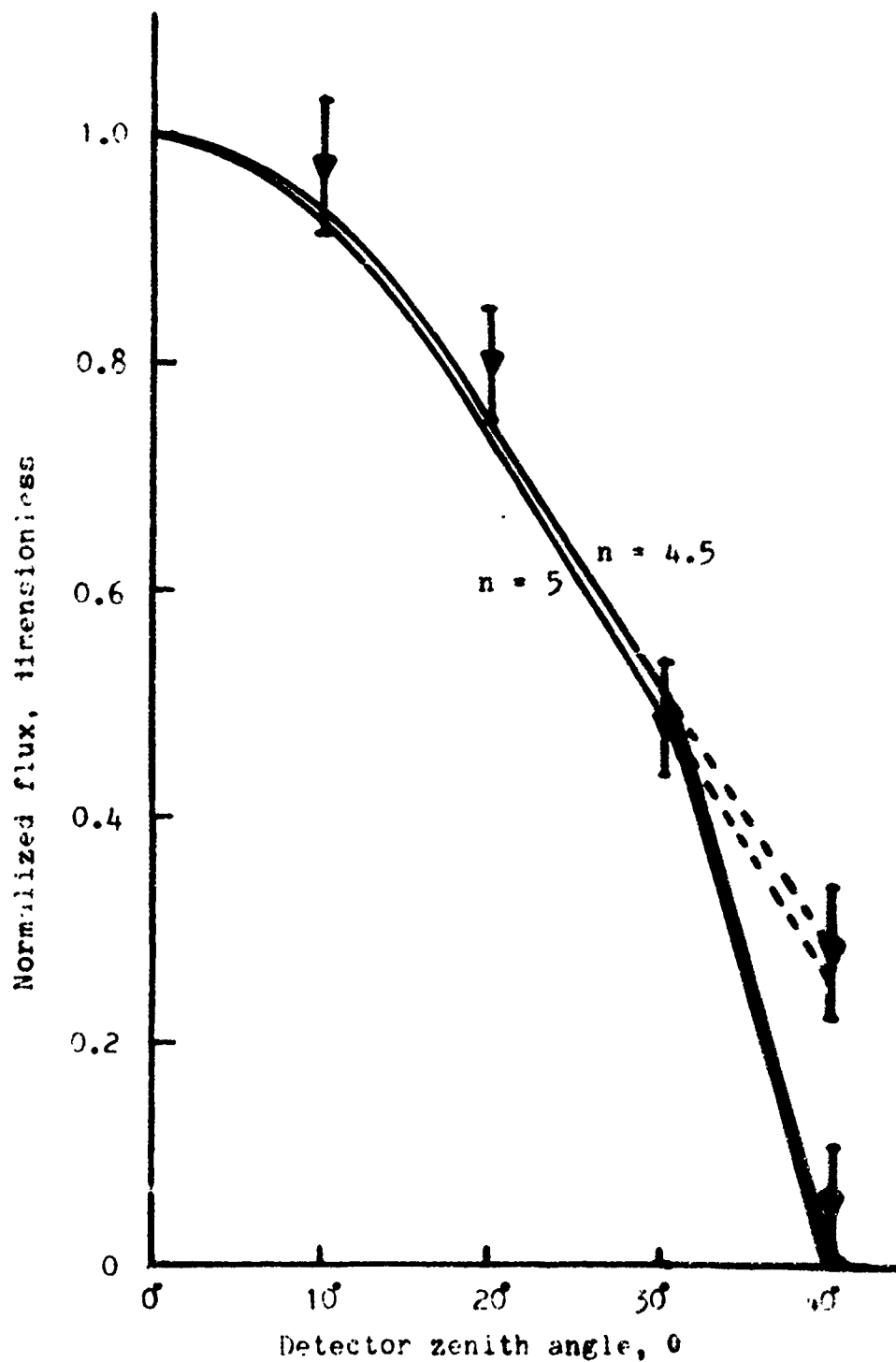


Figure 25. Comparison of predictions from program to measured rates in north half-plane (curve extrapolated to 40° NE), for $n = 4.5$ and $n = 5$. Calculation of rates from raw data by program RESULTS.

at half-maximum of $46.0^\circ \pm 0.5^\circ$, taking the value of n to be 4.7 ± 0.5 ; and

-- an average zenith-angle secant for the particles detected of 1.19, which is important in energy computations.

B. Description of the Stopping-Muon Flux at Sea Level

The value of the cosine-power n for stopping muons, as obtained in this experiment, is significantly higher than the cosine-powers of the differential muon energy spectra observed by other experimenters. For example, Kraushaar, in 1949, measured the muon differential range spectrum for $R > 71 \text{ gm cm}^{-2}$ of air (corresponding to a kinetic energy of about 350 MeV), and found n to be approximately 3.3.⁽¹³⁾ Zar, in 1951, measured the differential range spectrum for through particles in approximately the same energy band, and found n to be 2.97.⁽¹⁴⁾ Moroney and Parry, in 1954, also obtained an n of about 3.3 for the differential spectrum at 0.3 BeV/C.⁽³⁾ By contrast, the cosine-power of stopping muons as determined in this work was 4.7 ± 0.5 .

Several factors contribute to this difference. First, all of the other observers cited above used data as far away from the zenith as $\theta = 60^\circ$, whereas in this experiment no measurements beyond $\theta = 40^\circ$ were taken. The spectra in each of the cited works tends to dip until the zenith angle exceeds $\theta = 30^\circ$, when a leveling-off occurs; the average cosine-power over the entire range of zenith-angles is about 3 to 3.3, but the n in the regions nearer the zenith appears to be

somewhat greater. Second, the angular apertures of all of the telescopes in the cited works were somewhat wider than those of the ZADs in this experiment. Third, all of the telescopes used in the cited works were, to some degree, susceptible to enhancement by vertical showers as the telescopes were inclined to larger zenith angles. The latter consideration may be shown to be insignificant, however. When shower corrections were applied to the experimental data herein, the value of n at which S was minimized changed by less than 0.2; also, the cited experiments were consistent in their values of n independent of their shower susceptibility.

A fourth consideration in comparing the zenith-angle distributions is the energy band of the particles being counted. It is known that the cosine-power increases with decreasing energy, and that a stopping muon is of the minimum detectable energy at the earth's surface. The surrounding overburden also has an effect upon the energy distribution at the detector. More will be said about energy effects in the next section.

It is reasonable to state, however, that the flux description determined by this experiment,

$$I(\theta) = I_0 \cos^{4.7} \theta ,$$

is the relevant flux to employ in calculations concerning the wide-angle muon telescope described herein.

C. Energy Considerations

For a particle to stop in the detection system, it must pass

through three major contributors to ionization energy loss: the building roof and structure; the lead soft-component shield; and the scintillator of the stop tank. Figure 26 shows a cross-section of the building in which the detection system was maintained. For each of the paths shown, the average particle energy was calculated, using the following assumptions:

-- the muon specific energy losses in scintillating plastic and in carbon, expressed as $\text{MeV}\cdot\text{cm}^2/\text{gm}$, are approximately the same;

-- the muon specific energy losses in concrete and in copper are approximately the same; and

-- no scattering is assumed.

The results of these energy estimates were:

<u>Path Zenith Angle</u>	<u>Energy Loss Contribution</u>	<u>\overline{AE}</u>
0°	20 g/cm^2 plastic	70 MeV
	55 g/cm^2 lead	60 MeV
	90 g/cm^2 concrete	130 MeV
	TOTAL	260 MeV
30°	23 g/cm^2 plastic	80 MeV
	63 g/cm^2 lead	70 MeV
	104 g/cm^2 concrete	150 MeV
	TOTAL	300 MeV
40°	28 g/cm^2 plastic	100 MeV
	71 g/cm^2 lead	80 MeV
	450 g/cm^2 concrete	670 MeV
	TOTAL	850 MeV

The high energy-loss values in plastic are due to the sharp increase

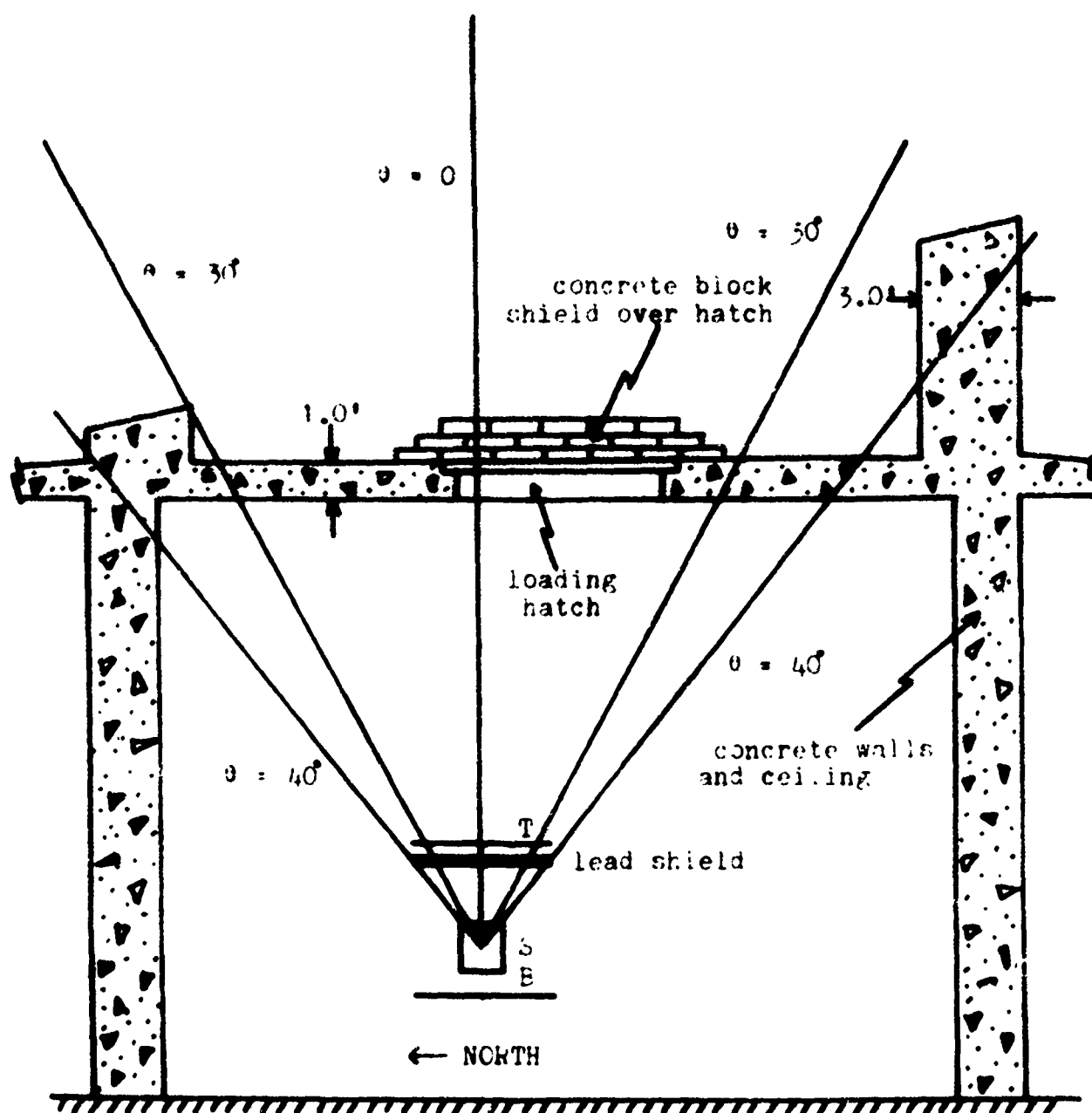


Figure 26. Stopping-muon telescope location within surrounding building (CMR building, Greenbury Point, U.S. Naval Radio Transmitter Station, Annapolis, Maryland.) A plywood-and-shingle roof covered the area between the two beveled columns shown, which are actually cross-sections through an octagonal structure 3.0 feet thick. Stopping power of concrete blocks through which vertical cosmic rays must pass may have been somewhat overestimated, since they are porous blocks, as opposed to the dense structural concrete elsewhere. Trajectories of 40° N and 40° S actually transit different amounts of concrete.

in $\frac{dE}{dx}$ as the muon stops. Range and energy-loss values were taken from High-Energy Particle Data, published by Lawrence Radiation Laboratory.

At first glance, the much higher energy required to produce a stopping muon with a zenith angle of 40° seems to imply that the surrounding building produces significant attenuation in the muon rate at $\theta = 40^\circ$. This would have artificially lowered the apparent cosine-power n . However, upon examining the differential sea-level muon spectra of Moroney and Parry⁽¹¹⁾, Kraushaar⁽¹²⁾, and Allkofer et al.⁽¹⁶⁾, there is no consistent difference in the differential intensities of muons of energy 260 MeV and those of 850 MeV. The spectra are very flat in this region, the greatest difference in the two intensities being about five percent. Thus, the effect of the building as shielding is merely to shift the energies of stopping muons to another portion of the energy spectrum, but not to decrease their number significantly.

D. Suggestions for Further Research

The following possibilities for further research were suggested by the results of this experiment and the problems associated therewith.

First, it is suggested that the zenith-angle distribution of stopping muons be measured at larger zenith angles. The only distribution of interest in this experiment was that which produced counts in the wide-angle muon telescope. However, any shallowing of the distribution at larger angles would be of great interest theoretically.

Second, an expression for the zenith-angle distribution should be developed which is a result of theoretical considerations. As stated previously, the use of the expression $I = I_0 \cos^n \theta$ is a customary, rather than a theory-based, procedure. A prediction of zenith-angle distribution should be associated with each muon production-attenuation model.

Third, a more extensive study of the incidence of shower-associated stopping muons should be undertaken. Most showers in this apparatus should have been eliminated by the anticoincidence plate; however, their persistence (due at least in part to the low efficiency of the bottom plate) may permit a study to be made of them. It is possible, also, that showers have distorted the apparent zenith-angle distribution in some way other than that assumed herein.

Fourth, a Monte Carlo calculation of scattering effects in the building and lead shielding should be undertaken. Muons of the energies being measured here are at least as susceptible to scattering as the through particles measured in other experiments, for which scattering corrections are often significant.

Finally, two areas of research have suggested themselves and are, although not directly related to zenith-angle distribution, infinitely related to the meaning and importance of stopping-muon cosmic rays at sea level. The first is the performance of a time-correlation of stopping-muon arrivals over an acceptance time of about one second. The ramifications of any non-random time peaks which might appear are manifold. Second, and lastly, a collection of shower-associated stopping-muon data should also be undertaken,

in solar and sidereal time. An ambiguity exists in the primary energy spectrum between 10^{13} eV and 10^{15} eV, and shower-associated stopping muons are in the ideal range for studying this ambiguity.

TABLE 1

Nuclear Abundances in the Primary
Cosmic Radiation (?)

<u>Element</u>	<u>Relative Abundance</u>
H	100
He	15
Be	0 to 0.4
C,N,O,F	1.2 ± 0.4
Ne	0.2
Mg	0.09
Si	0.07
Fe,Co,Ni	0.06
beyond Ni	$<10^{-5}$

TABLE 2

Major Dimensions of Detector System

Wide-Angle Stopping Muon Telescope

Size of top and bottom plates	48.0" x 48.0"
Separation of plates	48.0"
Scintillator size in stop tank	16 3/4" x 16 3/4" x 15" (N-S)
Height of stop tank center from bottom plate upper surface	15.75"
Offset of stop tank center from centerline of plates	0.5" to the south

Zenith-Angle Detectors and Mount

Size of ZAD scintillator	2.0" x 5.0" dia.
Radius of mount	60.0"
Radius of travel of ZAD scintillator centers	63.0"
Center of mount arc from center of stop tank	0 + 0.5" vertical, 0 + 0.5" E-W, 0.5" + 0.5" to the south
Height of vertical ZAD scintillator from top plate upper surface	30.5"

TABLE 3
ZADRESP3 Predictions of Normalized
ZAD Stopping-Muon Count Rates*

ZAD Position	<u>n, in $I = I_0 \cos^n \theta$</u>						
	<u>2.5</u>	<u>3.0</u>	<u>3.5</u>	<u>4.0</u>	<u>4.5</u>	<u>5.0</u>	<u>5.5</u>
10° N	.9597	.9519	.9441	.9365	.9290	.9216	.9143
10° S	.9597	.9519	.9441	.9365	.9290	.9216	.9143
20° N	.8498	.8231	.7974	.7726	.7488	.7258	.7037
30° N	.6891	.6407	.5960	.5547	.5165	.4812	.4485
30° E	.6857	.6380	.5940	.5533	.5157	.4809	.4488
30° S	.6764	.6286	.5844	.5436	.5059	.4710	.4388
40° N	.0456	.0379	.0315	.0262	.0218	.0181	.0151
40° NE	.5008	.4384	.3842	.3371	.2961	.2604	.2292
40° SE	.4929	.4313	.3778	.3313	.2908	.2556	.2249
40° S	.0232	.0191	.0158	.0131	.0108	.0090	.0074

* The program ZADRESP3 actually calculated absolute count rates, in terms of I_0 . The absolute rates were then normalized by division by the predicted rate of a tube at (0°,0°).

TABLE 4

Measured ZAD Counts, Normalized Rates, and
Unbiased Estimates of Error*

ZAD Position	Raw Data, $\frac{N}{N_0}$	Reciprocity Normalized Rate, $\frac{R(z)}{N_0}$	Estimated Error, \pm
10° N	$\frac{986}{894} , \frac{1013}{1185}$.971	$\pm .059$
10° S	$\frac{1112}{1185} , \frac{734}{714}$.982	$\pm .063$
20° N	$\frac{1071}{1036} , \frac{571}{740} , \frac{831}{1276}$.804	$\pm .051$
30° N	$\frac{534}{894} , \frac{301}{595}$.550	$\pm .046$
30° E	$\frac{292}{624} , \frac{333}{612}$.505	$\pm .047$
30° S	$\frac{698}{1276} , \frac{208}{356}$.565	$\pm .051$
40° N	$\frac{48}{395} , \frac{35}{356}$.109	$\pm .021$
40° NE	$\frac{178}{714} , \frac{200}{599}$.289	$\pm .031$
40° SE	$\frac{169}{612} , \frac{155}{610}$.265	$\pm .030$
40° S	$\frac{62}{595} , \frac{50}{624}$.091	$\pm .015$

*None of the corrections discussed in Sections IV D through IV G have been applied to either the rates or the error estimates.

TABLE 5

Summary of Corrections to be
Made to Data

<u>ZAD Position</u>	<u>Additive Correction to Rate</u>	<u>Source</u>	<u>Multiplicative Correction to σ</u>	<u>Source</u>
30° N	- .064	Showers	1.2	Shower rate uncertainty
30° E				
30° S				
40° N	- .024	Showers	3.9	Shower, false count, and position uncertainties
	- .022	Correlated pulsing		
	- .046	NET		
40° NE	- .024	Showers	2.0	Shower and top plate efficiency uncertainties
	+ .022	Top plate eff.		
	- .002	NET		
40° SE	- .024	Showers	2.0	Shower and top plate efficiency uncertainties
	+ .025	Top plate eff.		
	+ .001	NET		
40° S	- .024	Showers	3.9	Shower, false count, and position uncertainties
	- .018	Correlated pulsing		
	- .042	NET		

Literature Cited

- ¹ E.C. Ray, in Handbuch der Physik, vol. XLVI/1, Cosmic Rays I, ed. S. Flugge (Springer-Verlag, Berlin, 1961), p. 133.
- ² P. Morrison, in Handbuch der Physik, XLVI/1, p.5.
- ³ J. R. Moroney and J. K. Parry, Austral. J. Phys. 7, 3, 425. (1954)
- ⁴ G. Brooke, M.A. Meyer, and A.W. Wolfendale, Proc. Phys. Soc. (GB) 83, 5, 871. (1964)
- ⁵ N. Barash-Schmidt et al, Review of Particle Properties, January 1969 Edition (UCRL-8030 Pt. 1, Lawrence Radiation Laboratory, Berkeley, Calif., 1969), pp. 24-25.
- ⁶ B. Rossi, Cosmic Rays (McGraw-Hill, New York, 1964)
- ⁷ R. Turner, C.M. Ankenbrandt, and R.C. Larsen, Phys. Rev. D 4, 17. (1971)
- ⁸ J. L. Zar, Phys. Rev. 83, 4, 761. (1951)
- ⁹ J. N. Crookes and B.C. Rastin, Nuc. Phys. B 39, 493. (1972)
- ¹⁰ J.R. Winckler and W.G. Stroud, Phys. Rev. 76, 8, 1012. (1949)
- ¹¹ C.T. Brown, "An Experimental Study of Certain Neutral Cosmic Ray Interactions," Doctoral Thesis, Georgia Institute of Technology, 1972, p. 64.
- ¹² J.R. Wolberg, Prediction Analysis (D. Van Nostrand, Princeton, 1967), pp. 32 ff.

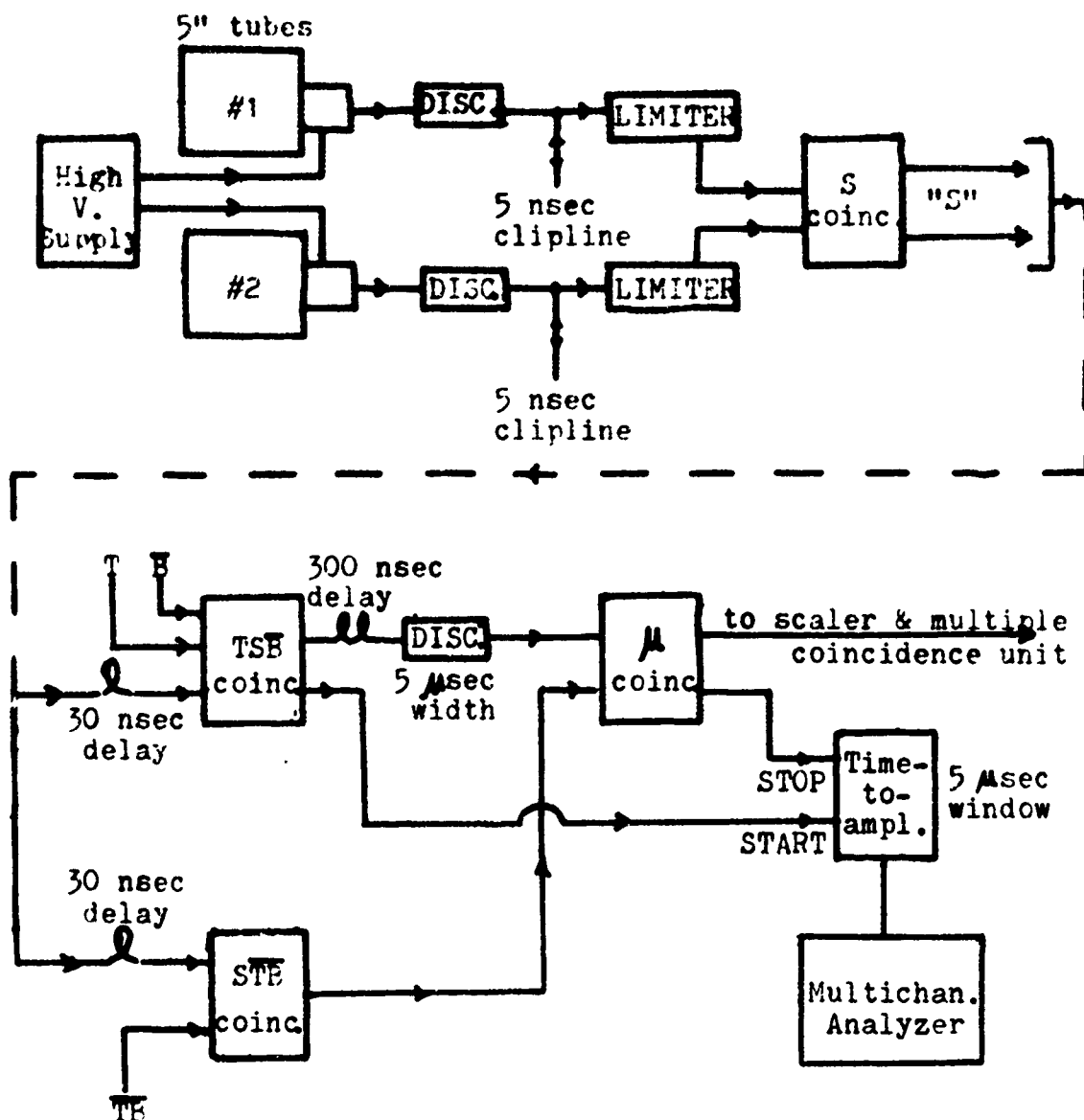
Literature Cited (Cont'd)

- ¹³ W. L. Kraushaar, Phys. Rev. 76, 1045. (1949)
- ¹⁴ J. L. Zar, Phys. Rev. 83, 761. (1951)
- ¹⁵ High-Energy Particle Data, vol. II, Range-Energy and dE/dx Data of Charged Particles in Matter (UCRL-2426, Lawrence Radiation Laboratory, Berkeley, Calif., 1966).
- ¹⁶ O. C. Allkofer, W. D. Dau, and H. Jokisch, Phys. Lett. 22, 606. (1967).

APPENDIX A

Muon Telescope and ZAD Circuitry

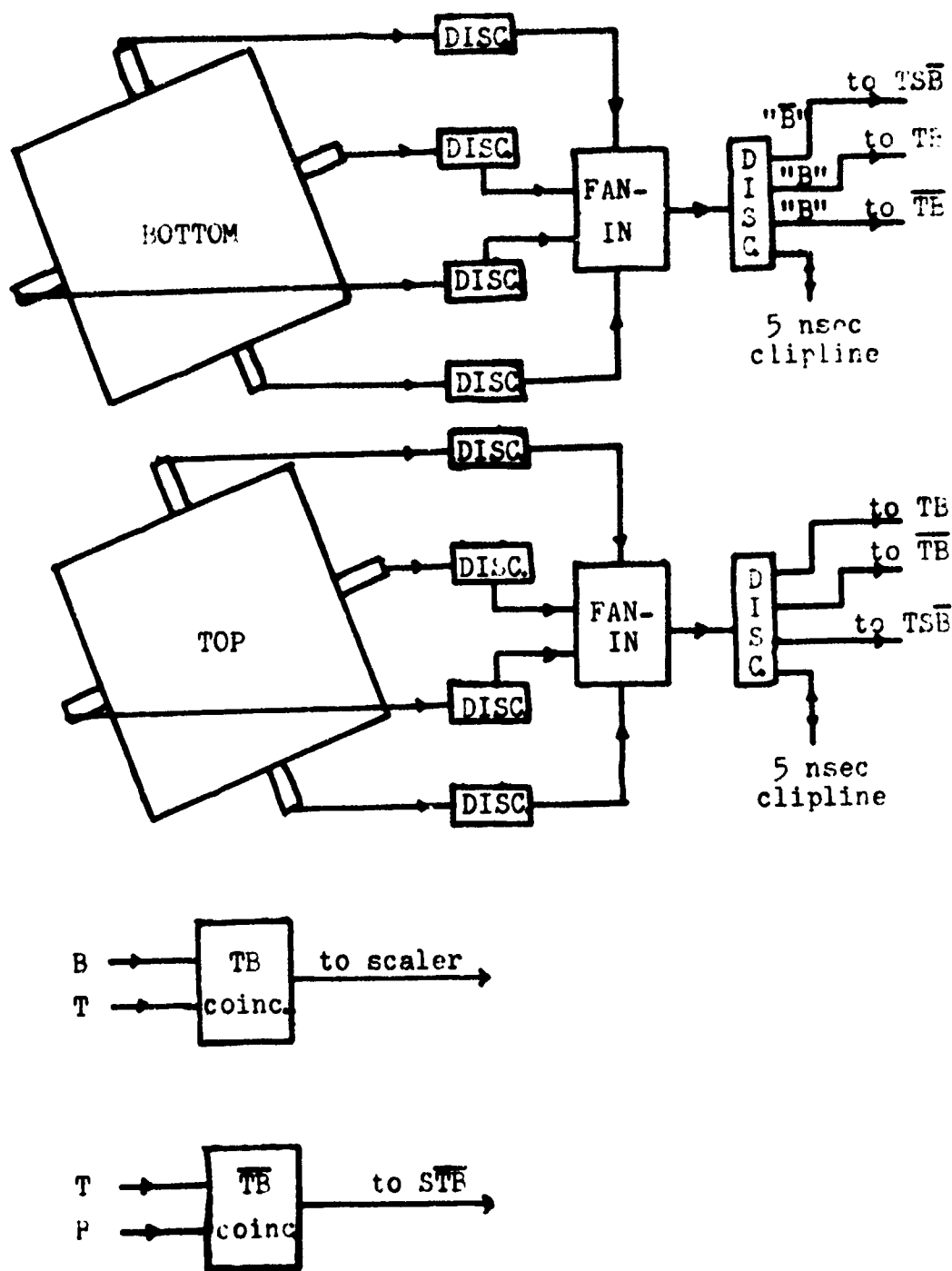
The following three pages contain the block diagrams of the electronic components of the wide-angle muon telescope and the zenith-angle detectors, exclusive of the circuitry for the automatic data output system. The high-voltage supplies are omitted from the plate circuitry and ZAD circuitry. Separate high-voltage supplies are used for the stop tank tubes (2200 v or 2300 v), top and bottom plate tubes (2200 v), and zenith-angle detector tubes (1600 v).

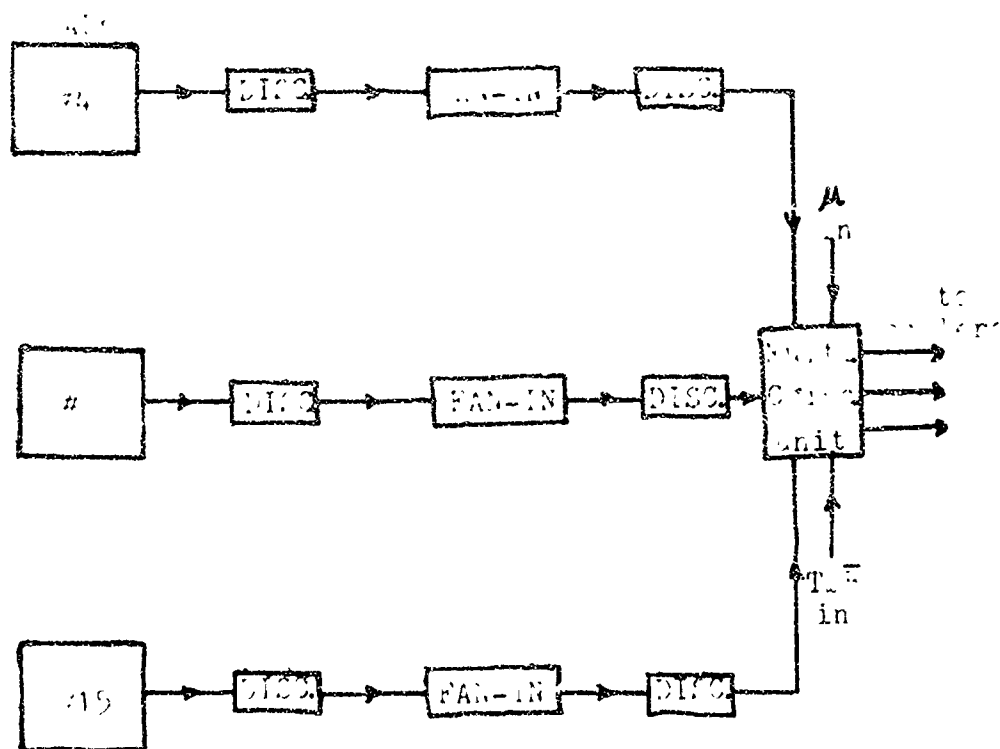


Circuitry of stop tank, and of muon identification. Note:

1. High voltage supply to stop tank tubes separate from that of top and bottom plates.
2. Cliplines cause a pulse-shortening by reflection, giving an effective resolving time of 5 nsec between 5" tubes.
3. Limiters do not function as such, remain in circuit only to preserve timing (after 1 February 1975).
4. 300 nsec delay causes all "muons" decaying between 0.5 and 5.5 sec to register a count. The time-integral of the muon decay curve over this interval yields an automatic efficiency of 78%.

Top and Bottom Plate Circuitry





APPENDIX B

Zenith-Angle Detector Rate-Predictive Programs

The following pages list the predictive computer programs described in Section III B, and contain some sample runs of these programs. The programs ZADRESP, ZADRESP2 and ZADRESP3 represent a developmental sequence, and are presented in chronological order. ZADWRITE is used to feed the coordinates of the subdivisions of a ZAD into a file, named ZADCOORD, from which they may be read by ZADRESP2 or ZADRESP3.

ZAADRESP

```

10      80 PRINT "INPUT N...";
11      90 INPUT N
12      110 PRINT "INPUT ZETA,XI...";
13      120 INPUT E,A
14      130 LET D=1
15      131 LET T=2
16      140 LET X(D)=60*SIN(E/57.29)*COS(A/57.29)
17      150 LET Y(D)=60*SIN(E/57.29)*SIN(A/57.29)
18      160 LET Z(D)=60*COS(E/57.29)
19      170 LET R(D)=60
20      180 FOR X=-7.5 TO 7.5
21      190 FOR Y=-7.5 TO 7.5
22      200 FOR Z=-7.5 TO 7.5
23      201 LET X(T)=X+(X(D)-X)*(33.5-Z)/(Z(D)-Z)
24      202 LET Y(T)=Y+(Y(D)-Y)*(33.5-Z)/(Z(D)-Z)
25      203 IF X(T)>24 THEN 260
26      204 IF X(T)<-24 THEN 260
27      205 IF Y(T)>24 THEN 260
28      206 IF Y(T)<-24 THEN 260
29      210 LET R=SQR((X(D)-X)^2 + (Y(D)-Y)^2 + (Z(D)-Z)^2)
30      220 LET U=X(D)*(X(D)-X) + Y(D)*(Y(D)-Y) + Z(D)*(Z(D)-Z)
31      230 LET Q=(Z(D)-Z)/R
32      240 LET P=U/((R^3)*R(D))
33      250 LET C=C+(Q^N)*P
34      260 NEXT Z
35      270 NEXT Y
36      280 NEXT X
37      290 PRINT "RATE =" ;C;"TIMES I(0)*SIGMA."
38      999END

```

READY

/OLD ZADRESP/ROU

2) ZADRESP 12 MAY 75 23:00

INPUT N...? 4.7

INPUT ZETA,XI...? 0,0

RATE = 1.105 TIMES I(0)*SIGMA.

9.233 SEC. 26 I/O

2)READY

ROU

ZADRESP 12 MAY 75 23:01

INPUT N...? 4.7

INPUT ZETA,XI...? 40,45

RATE = 0.327894 TIMES I(0)*SIGMA.

9.275 SEC. 26 I/O

READY

* * * * *

GENERATION OF A NORMALIZED COUNT AT 40 DEGREES NORTH-EAST USING PROGRAM "ZADRESP". THE ACTUAL NORMALIZATION TAKES PLACE BY DIVIDING THE TWO ABSOLUTE RATES. NOTE THE DIFFERENCE OF A CONSTANT BETWEEN THESE ABSOLUTE RATES AND THOSE OF "ZADRESP3". THE "ZADRESP3" VALUES ARE CORRECT.

ZADCOORD

```

150 LET D=1
155 LET T=2
157 LET R(D)=.68
190 FILE#1:"ZADCOORD"
195 PRINT "INPUT EXPONENT OF COS(THETA)...";
197 INPUT N
200 FOR L=1 TO 16
210 READ #1: X(D)
220 FOR X=-7 TO 7 STEP 2
230 FOR Y=-8 TO 8 STEP 2
240 FOR Z=-8 TO 8 STEP 2
241 LET X(T)=X + (X(D)-X)*(33.5-Z)/(Z(D)-Z)
242 LET Y(T)=Y+(Y(D)-Y)*(33.5-Z)/(Z(D)-Z)
243 IF X(T)<=-23 THEN 300
245 IF X(T)>25 THEN 300
246 IF Y(T)<=-24 THEN 300
247 IF Y(T)>24 THEN 300
248 LET R=SQR((X(D)-X)^2 + (Y(D)-Y)^2 + (Z(D)-Z)^2)
250 LET U=X(D)*(X(D)-X)+Y(D)*(Y(D)-Y)+Z(D)*(Z(D)-Z)
270 LET Q=(Z(D)-Z)/R
280 LET P=U/(R^3)*R(D)
290 LET C=C+(X^N)*P/16
300 NEXT Z
310 NEXT Y
320 NEXT X
330 NEXT L
340 PRINT C
999END

```

NOTE: THE PROCEDURE FOR OBTAINING NORMALIZED COUNTS FROM "ZADRESP2" AND "ZADRESP3" ARE IDENTICAL. THEREFORE, A SEPARATE SAMPLE RUN OF "ZADRESP2" AND "ZADWRITE" IS NOT INCLUDED. "ZADRESP2" USES THE SAME DETECTOR MEASUREMENTS AS DOES "ZADRESP3", BUT DOES NOT PROVIDE AS MUCH INFORMATION.

ZADCCORD

```

1 LET D=1
2 LET R=0.05
3 FILE #1:"ZADCCORD"
4 PRINT "INPUT NORMALIZING FACTOR";
5 INPUT C
7 REM THE NEXT STEP IS DUFFY IF ZADCCORD IS USED
8 PRINT "INPUT DETECTOR ZENITH, AZIMUTH...";
9 INPUT Z,A
10 PRINT "INPUT EXPONENT OF ZENITH-ANGLE DIST...";
11 INPUT N
20 REM LINES 30-90 ALSO DUFFY IF ZADCCORD USED
30 LET X1=R*(C)*SIN(E/57.29)*COS(A/57.29)+0.5
40 LET Y1=R*(C)*SIN(E/57.29)*SIN(A/57.29)
50 LET Z1=R*(C)*COS(E/57.29)
60 READ #1:X1,Y1,Z1
70 FOR X4=-7 TO 7 STEP 2
80 FOR Y4=-8 TO 8 STEP 2
90 LET R2=R*((X1-X4)^2 + (Y1-Y4)^2 + (Z1-Z4)^2)
100 LET X2=X4+(X1-X4)*(Z2-Z4)/(Z1-Z4)
110 LET Y2=Y4+(Y1-Y4)*(Z2-Z4)/(Z1-Z4)
120 IF X2<-23.5 THEN GOTO 210
130 IF X2>24.5 THEN GOTO 210
140 IF Y2<-24 THEN GOTO 210
150 IF Y2>24 THEN GOTO 210
160 LET Z3=0.575
170 LET X3=X4+(X1-X4)*(Z3-Z4)/(Z1-Z4)
180 LET Y3=Y4+(Y1-Y4)*(Z3-Z4)/(Z1-Z4)
190 LET D=D+0.5*(X3-X4)^2 + (Y3-Y4)^2 + (Z3-Z4)^2
200 LET C=C+0.5*15.62/15*( (Z1-Z4)/R )^4/(C^2)
210 NEXT Y4
220 NEXT X4
230 LET C=D+1
240 IF C<15 THEN GOTO 25
250 PRINT "AVERAGE RANGE THROUGHOUT :";C;" INCHES."
260 PRINT "COUNT RATE :";C;" TIMES 1000 SIG/SEC."
270 PRINT "Z :"; ZENITH ANGLE.
280 END

```

/OLD ZADWRITE/RUN/OLD ZADRESP3/RUN

2) ZADWRITE 12 MAY 75 22:32

INPUT DETECTOR ZENITH, AZIMUTH ANGLES...? 0,0

4) ZADRESP3 12 MAY 75 22:32

INPUT NORMALIZING FACTOR? 1

INPUT DETECTOR ZENITH, AZIMUTH...? 0,0

INPUT EXPONENT OF ZENITH-ANGLE DIST...? 4.7

AVERAGE RANGE TRAVERSED = 8.42407 INCHES.

COUNT RATE = 25.0236 TIMES $1(0)*\text{SIGMA}$.

25.0236 = NORMALIZED RATE.

27.976 SEC. 60 I/O

4) READY

/OLD ZADWRITE/RUN/OLD ZADRESP3/RUN

2) ZADWRITE 12 MAY 75 22:37

INPUT DETECTOR ZENITH, AZIMUTH ANGLES...? 40,45

4) ZADRESP3 12 MAY 75 22:37

INPUT NORMALIZING FACTOR? 25.0236

INPUT DETECTOR ZENITH, AZIMUTH...? 40,45

INPUT EXPONENT OF ZENITH-ANGLE DIST...? 4.7

AVERAGE RANGE TRAVERSED = 10.7775 INCHES.

COUNT RATE = 7.03727 TIMES $1(0)*\text{SIGMA}$.

.281225 = NORMALIZED RATE.

27.504 SEC. 60 I/O

4) READY

* * * * *

GENERATION OF A NORMALIZED COUNT AT 40 DEGREES NORTH-EAST USING PROGRAM "ZADRESP3".

ZADWRITE

```
1 FILE #1:"ZADCOORD"  
2 SCRATCH #1  
5 LET D=1  
10 LET R(D)=63.0  
15 PRINT "INPUT DETECTOR ZENITH, AZIMUTH ANGLES...";  
20 INPUT E  
25 IF E=0 THEN 200  
30 LET E=E/57.29  
40 LET A=A/57.29  
50 LET X0=R(D)*SIN(E)  
51 LET X0=X0+C.5  
80 LET D1=1.1*COS(E)  
85 LET D2=1.1  
130 FOR X1=X0-1.5*D1 TO X0+1.5*D1 STEP D1  
140 FOR Y1=-1.5*D2 TO 1.5*D2 STEP D2  
150 LET Z=SQR(R(D)^2 - X1^2 - Y1^2)  
152 LET W=ATN(Y1/X1)  
154 LET R1=SQR(X1^2+Y1^2)  
156 LET Y=R1*SIN(W+A)  
158 LET X=R1*COS(W+A)  
160 WRITE #1:X  
170 NEXT Y1  
180 NEXT X1  
190 STOP  
200 LETZ=63.0  
210 FOR X=-1.15 TO 2.15 STEP 1.1  
220 FOR Y=-1.65 TO 1.65 STEP 1.1  
230 WRITE #1:X  
240 NEXT Y  
250 NEXT X  
999 END
```

APPENDIX C

Muon Telescope Analysis Programs

Program MURESP is a direct offshoot of the ZADRESP3 program. The only change in detector description is the replacement of the ZAD area and solid angle with the subdivisions of the top plate. A factor of \cos is required due to the top plate's oblique angle with respect to the incoming flux away from the vertical

Programs DETECTOR, whose detector dimensions are only approximate, and DETECTR2, where the dimensions are considered accurate to $\pm 0.5''$, are the products of the "trajectory" method of predicting detector response. They are not suitable for verification by zenith-angle detectors, as is MURESP. However, they employ the same detector description as does MURESP; further, multiplying the curve in Figure 15 by $I(\theta, \phi) \sin \theta$ and integrating over the wide-angle telescope aperture should give the same results that MURESP gives.

MURLESF

```
10 PRINT "INPUT EXPONENT OF INCOEFFICIENTS"
15 INPUT N
17 PRINT "SOUTH HALF(1) OR NORTH HALF(2)"
20 INPUT H
22 IF H=2 THEN 27
23 LET A=-20.5
24 LET B=-2.5
25 GOTO 30
27 LET A=3.5
28 LET B=21.5
30 LET Z1=32.25
40 FOR X1=A TO B STEP 6
50 FOR Y1=-21 TO 21 STEP 6
60 FOR X2=-7 TO 7 STEP 2
70 FOR Y2=-8 TO 8 STEP 2
80 FOR Z2=-8 TO 8 STEP 2
90 LET R=SQRT((X2-X1)^2 + (Y2-Y1)^2 + (Z2-Z1)^2)
100 LET C=(Z1-Z2)/R
110 LET D=8*36*(C^(N+1))/(R^2)
120 LET T=T+D
130 IF C<COS(10/57.29) THEN 160
140 LET F(1)=F(1)+D
150 GOTO 300
160 IF C<COS(20/57.29) THEN 190
170 LET F(2)=F(2)+D
180 GOTO 300
190 IF C<COS(30/57.29) THEN 220
200 LET F(3)=F(3)+D
210 GOTO 300
220 IF C<COS(40/57.29) THEN 250
230 LET F(4)=F(4)+D
240 GOTO 300
250 LET F(5)=F(5)+D
300 LET G1=G1+1/C
310 LET S=S+1
320 NEXT Z2
330 NEXT Y2
340 NEXT X2
350 NEXT Y1
360 NEXT X1
37 PRINT
```

CONTINUED

MURESP (CONTINUED)

```
370 PRINT "TOTAL COUNT RATE ="; T; "TIMES 100 * SIGMA."  
380 PRINT  
385 PRINT "LOWER BOUND", "UPPER BOUND", "COUNTS WITHIN"  
390 FOR L=1 TO 5  
400 PRINT 10*(L-1), 10*L, F(L)  
410 NEXT L  
420 PRINT  
430 PRINT "AVERAGE SECANT ="; W1/S  
999END
```

DETECTION

```

5 PRINT "INPUT VOLUME ELEMENT SIZE...";
6 INPUT S
10 DIM A(15)
12 PRINT "INPUT THETA...";
16 INPUT T
18 LET D:1/2 + 1
19 FOR P=0 TO 350 STEP 1
20 FOR X0=-8 TO 8-S STEP S
30 FOR Y0=-8 TO 8-S STEP S
40 FOR Z0=0 TO 16-S STEP S
70 LET X=X0 + S/2 + (44-Z0-S/2)*TAN(T/17.29)*COS(P/17.29)
80 LET Y=Y0 + S/2 + (44-Z0-S/2)*TAN(T/17.29)*SIN(P/17.29)
90 IF X<-24 THEN 200
100 IF X>24 THEN 200
110 IF Y<-24 THEN 200
120 IF Y>24 THEN 200
150 LET A(D)=A(D)+1
200 NEXT Z0
230 NEXT Y0
240 NEXT X0
250 NEXT P
260 PRINT A(3)*100/((16/S)^3)
999 END

```

DETECTING

```

10 PRINT "HIGH ZENITH ANGLE":
20 INPUT E
30 FOR A=0 TO 340 STEP 20
40 FOR X2=-7 TO 7 STEP 2
50 FOR Y2=-8 TO 8 STEP 2
60 FOR Z2=-8 TO 8 STEP 2
70 LET X1=X2+(32.25-Z2)*TAN(E/57.29)*COS(A/57.29)
80 LET Y1=Y2+(32.25-Z2)*TAN(E/57.29)*SIN(A/57.29)
90 IF X1<-23.5 THEN 140
100 IF X1>24.5 THEN 140
110 IF Y1<-24 THEN 140
120 IF Y1>24 THEN 140
130 LET C=C+1
140 NEXT Z2
150 NEXT Y2
160 NEXT X2
17 NEXT A
18 PRINT "RELATIVE DETECTION ABILITY ";C
99 END

```

APPENDIX D

Statistical Analysis Program

Program RESULTS, listed in the following pages, has two output forms. First, it may be used to print out a table of reciprocity-normalized data points, corrected or uncorrected, along with the estimated errors and the raw numbers of counts. Second, it can evaluate the flat and weighted S values for the predicted data listed in lines 400-410, for either corrected or uncorrected data. The S values generated by excluding the points at 40° N and 40° S may be obtained by the following modification:

320 DATA 8

560

590

410 DATA (predictions for 40° NE, 40° SE only)

RESULTS

```

1 DIM A(20),B(20),C(20),D(20),E(20),F(20),P(20),S(20)
2 PRINT "Z=0"
3 MAT F=CON
4 PRINT "CONNECTED(1) OR UNCONNECTED(2) ";
5 INPUT G
6 READ N
7
8 READ L,Y,Z
9 IF L=1 THEN 25
10 IF G=2 THEN 15
11 LET E(L)=Y
12 LET F(L)=Z
13 GOTO 15
14 FOR L=1 TO N
15 READ P(L)
16 NEXT L
17 FOR L=1 TO N
18 IF L=3 THEN 1100
19 READ A(L),B(L),C(L),D(L)
20 LET A=A(L)
21 LET B=B(L)
22 LET C=C(L)
23 LET D=D(L)
24 LET R(L)=SQR(A*A+B*B+C*C+D*D)
25 LET R(L)=R(L)+E(L)
26 LET EI=SQR(1+1/SQR(A)+1/SQR(B)+1/SQR(C)+1/SQR(D))-1
27 LET Z=1-SQR(1-1/SQR(A)-1/SQR(B)-1/SQR(C)-1/SQR(D))
28 LET S(L)=R(L)*EI*F(L)
29 LET W=W+(R(L)-P(L))*Z/(S(L)*Z)
30 LET CI=CI+SQR(B(L)*D(L))*(R(L)-P(L))*Z/P(L)
31 NEXT L
32 PRINT "DO YOU WANT TABLE(1) OR CI+SQUARED(2) ";
33 INPUT G
34 IF G=2 THEN 300
35 PRINT "RECIPROCALITY"
36 PRINT "RAW DATA", "NORMALIZED"
37 PRINT "POSITION", "W/N.C.", "RATE", "SIGMA"
38 PRINT "-----", "-----", "-----", "-----"
39 FOR L=1 TO N
40 READ L3
41 PRINT A(L);"/";B(L)
42 IF L=3 THEN 1250

```

(CONTINUED)

RESULTS (CONTINUED)

```

230 PRINT L3, A2, L3
235 PRINT, C(L);
240 PRINT
250 NEXT L
260 PRINT
270 STOP
300 PRINT "WEIGHTED S = "; W
310 PRINT "FLAT S = "; C1
320 DATA 10
340 REM NEXT SIX LINES ARE (POSITION, RATE CORR., SID A, S
350 DATA 4, -.064, 1.2
351 DATA 5, -.064, 1.2
352 DATA 6, -.064, 1.2
353 DATA 7, -.046, 3.5
354 DATA 8, -.062, 2.0
355 DATA 9, .001, 2.0
356 DATA 10, -.042, 3.9
357 DATA -1, -1, -1
359 REM DATA IS FOR A14.0
400 DATA .965, .335, .7726, .5547, .7733, .5416
410 DATA .0261, .3571, .7313, .0151
420 DATA 966, 894, 1613, 1100, 10 M
430 DATA 1112, 1185, 754, 714, 10 S
440 DATA 1071, 1056, 801, 1276, 571, 740, 10 W
450 DATA 534, 894, 351, 555, 30 S
460 DATA 292, 524, 335, 612, 30 E
470 DATA 696, 1276, 208, 355, 30 S
480 DATA 48, 395, 35, 355, 40 W
490 DATA 178, 714, 200, 599, 40 NE
500 DATA 169, 612, 155, 810, 40 SE
510 DATA 62, 595, 50, 624, 40 S
1000 DATA "10 N", "10 S", "20 N", "30 N", "30 E", "30 S"
1010 DATA "40 N", "40 SE", "40 SW", "40 S"
1100 READ A, B, C, D, E, F
1110 LET R(3) = ((A*B+C*D)/(B*D+F))^(1/3)
1120 LET EI = 1 + 1/SQR(A) + 1/SQR(B) + 1/SQR(C)
1125 LET EI = EI + 1/SQR(D) + 1/SQR(E) + 1/SQR(F)
1130 LET EI = EI^(1/3) - 1
1140 LET A(3) = A
1150 LET B(3) = B
1160 LET C(3) = C
1170 LET D(3) = D
1200 GOTO 110
1250 PRINT L3, A; "/"; B, C(L), D(L)
1260 GOTO 230
9999 END

```